



HAL
open science

Nanoscale Seebeck effect at hot nanostructures

Aboubakry Ly

► **To cite this version:**

Aboubakry Ly. Nanoscale Seebeck effect at hot nanostructures. Micro and nanotechnologies/Microelectronics. Université de Bordeaux, 2018. English. NNT: 2018BORD0010. tel-01841492

HAL Id: tel-01841492

<https://theses.hal.science/tel-01841492>

Submitted on 17 Jul 2018

HAL is a multi-disciplinary open access archive for the deposit and dissemination of scientific research documents, whether they are published or not. The documents may come from teaching and research institutions in France or abroad, or from public or private research centers.

L'archive ouverte pluridisciplinaire **HAL**, est destinée au dépôt et à la diffusion de documents scientifiques de niveau recherche, publiés ou non, émanant des établissements d'enseignement et de recherche français ou étrangers, des laboratoires publics ou privés.

THÈSE

présentée à

UNIVERSITÉ DE BORDEAUX

ÉCOLE DOCTORALE DE SCIENCES PHYSIQUES ET DE L'INGÉNIEUR

par **Aboubakry LY**

POUR OBTENIR LE GRADE DE

DOCTEUR

SPÉCIALITÉ : Lasers, Matière et Nanosciences

**Effet Seebeck à l'échelle nanométrique de
nanostructures chaudes**

soutenue le 09 Février 2018 devant le jury composé de

M	Frank CICHOS	Professeur, Universität Leipzig	Rapporteur et Président
M	Manoel MANGHI	Maître de Conférences, Université de Toulouse	Rapporteur
M	Thomas BICKEL	Maître de Conférences, Université de Bordeaux	Examineur
M	Alois WÜRGER	Professeur, Université de Bordeaux	Directeur de Thèse

Thèse préparée à l'Université Bordeaux 1
au Laboratoire Ondes et Matière d'Aquitaine (LOMA), UMR5798,
351 cours de la Libération, 33405 Talence cedex.

Nanoscale Seebeck effect at hot nanostructures

Abstract

The aim of this work is to study the nanoscale Seebeck effect at hot nanostructures. At first, we study the thermo-electrophoresis self-propulsion mechanism for a heated metal capped Janus colloid. The self-propulsion mechanism is mainly induced by the electrolyte Seebeck effect or thermoelectric effect. This effect takes its origin from the separation of charges occurring while a temperature gradient is present in a electrolyte solution: A strong absorption of laser light by the metal side of the particle creates a temperature gradient which in turn acts on ion-species (positive and negative) and drives them to the hot or the cold region. This motion of ion results in a dipolar electric field which, close to the particle, depends strongly on the surface properties. The change of behavior of the electric field at the insulating or conducting surface does not affect the velocity of the particle. At second, we study the effect of hydrodynamic interactions and counterion condensation in thermophoresis for DNA polymer. As the main result, the thermophoretic mobility shows, in function of the chain length, a non-monotonous behavior and consists of two contributions induced by the dominant driving forces which are the thermally induced permittivity-gradient and the electrolyte Seebeck effect. At the end, we compare our theoretical result with recent experiment on single-stranded DNA.

Keywords: thermophoresis, temperature gradient, self-propulsion, Janus colloid, permittivity gradient, DNA, Seebeck effect, hydrodynamic.

Effet Seebeck à l'échelle nanométrique de nanostructures chaudes

Résumé

L'objectif de ce travail est d'étudier l'effet thermoélectrique à l'échelle nanométrique des nanostructures chauffées. Dans un premier temps, nous étudions les mécanismes d'autopropulsion thermo-électrophorétique de particules Janus chauffées par laser. Ce mécanisme d'autopropulsion est principalement induit par l'effet Seebeck ou l'effet thermoélectrique. Cet effet provient de la séparation des charges survenues lorsqu'un gradient de température est présent dans la solution d'électrolyte: Une forte absorption du laser par la partie métallisée de la particule génère un gradient de température qui en retour agit sur les espèces ioniques (positive et négative) et les conduit vers les zones chaudes ou les zones froides. Ce mouvement d'ions entraîne la création d'un champ électrique dipolaire qui, à proximité de la particule, dépend fortement des propriétés de surface. Ce changement de comportement de ce champ électrique sur une surface isolant ou conductrice n'affecte pas la vitesse de la particule. Dans un second temps, nous étudions les effets d'interactions hydrodynamiques et de la condensation des contre-ions sur la thermophorèse des polymères d'ADN. Comme résultat principal, la mobilité thermophorétique montre, en fonction de la longueur de la chaîne, un comportement non-monotone et se compose de deux contributions induites par les forces conductrices dominantes que sont l'effet Seebeck et le gradient de permittivité. À la fin, nous comparons notre résultat théorique avec une récente expérience sur l'ADN.

Mots clés: thermophorèse, gradient de température, auto-propulsion, particule Janus, gradient de température, ADN, effet Seebeck, hydrodynamique.

Contents

1	Introduction	5
1.1	Phoretic transport	5
1.2	Mechanisms	6
1.3	Motion in a temperature gradient	6
1.4	Summary	8
2	Electrolyte Seebeck effect	10
2.1	Seebeck effect in a 1-D geometry	10
2.2	Seebeck effect in 3-D system	12
2.2.1	ion current	12
2.2.2	Thermoelectric field and thermocharge	13
3	Nanoscale Seebeck effect	16
3.1	Introduction	16
3.2	Boundary layer approximation	17
3.2.1	Electrostatic boundary conditions	17
3.2.2	Temperature gradient at the particle surface	19
3.3	Seebeck effect: uncharged particle	20
3.3.1	Debye-Hückel approximation	20
3.3.2	Insulating particle	21
3.4	Charged surfaces	22
3.4.1	Poisson- Boltzmann theory	22
3.4.2	Charged insulating surface	23
3.4.3	Charged conducting surface	25
3.5	Hydrodynamic phoretic velocity	26
3.5.1	Slip-velocity	26

<i>CONTENTS</i>	4
3.5.2 Drift velocity	30
3.6 Results and discussion	32
3.6.1 Thermocharge and electric field	32
3.6.2 Polarization charge on the conducting surface	33
3.6.3 Granular gold surface	35
3.6.4 Comparison with experiment	36
3.7 Conclusion	37
4 Hydrodynamic interactions in DNA thermophoresis	38
4.1 Introduction	38
4.2 Thermodynamic forces	39
4.3 Hydrodynamic interactions	42
4.4 Counterion condensation	45
4.5 Results and comparison with experiment	46
4.6 Conclusion	53
5 Ion dynamics: time dependent effect	55
5.1 Charge conservation equation	55
5.2 Effect on Janus particle	56
5.3 Effect on thermophoresis	57
5.4 Conclusion	58
6 Summary and conclusion	60
A Seebeck effect of an uncharged particle	63
A.1 Equation for the ionic current	63
A.2 Debye-Hückel theory	64
A.3 Insulating particle	66
A.4 Conducting particle	67
B Poisson-Boltzmann theory	70
C Polarization charge	72
D Time dependent Seebeck effect	74
D.1 Temperature field	74
D.2 Conservation equation	75
D.3 Method of resolution	76

Chapter 1

Introduction

1.1 Phoretic transport

When applying an external force on microparticles suspended in a fluid, the system leads to a transport mechanism known as the name of *phoresis*. The concept of phoretic transport has been known for more than a century, and it's defined as a movement of colloidal particles caused by an applied external field. The most important property of phoretic transport is that there are no external force [1]. The motion arises from the action of the particle on the surrounding fluid. The phoretic movement of particle arises mainly from the interaction between the surface of the particle and its surrounding fluid or even with the various solutes solvent. This transport mechanism shows basic differences with the transport induced by body forces such as gravity, where the external field exerts a net force on the particle.

In the last few decades, the development of experimental techniques, studying the migration of particles under the influence of an gradient field, are strongly based on this phoretic transport phenomenon. Among these techniques, one can cite the field-flow fractionation method (FFF) which was first introduced by Giddings [2]. The FFF method consists of separating particles by applying a gradient field to a fluid suspension pumped trough a long channel. In this method, the separation of particles is caused, first, by the applied field which is perpendicular to the flow in the channel, and second by the differences in particle's phoretic mobility. In the same way, another experimental method, consisting of amplified migration of large particles in a solution through a channel, are developed more recently [3]. The phoresis mechanism has also brought a huge improvement in other trapping

techniques for colloidal particles [4] or for DNA [5], and constitute the key physical property when studying self-propulsion movement for microswimmers.

1.2 Mechanisms

Among the class of phoretic transport, the particles can move by electrophoresis, diffusiophoresis or thermophoresis. These possibilities consist of creating motion of a suspended microparticle by imposing a gradient field such as an electric field, a temperature gradient or a concentration gradient of small solutes surrounding the particle. The resulting transport mechanism refers to electrophoresis, thermophoresis, and diffusiophoresis, respectively. The electrophoresis mechanism is the most oldest one because it was established by Smoluchowski since 1905 [9], and later Keh and Anderson developed this concept by clarifying the role of the electrostatic boundary effects on the electrophoretic motion of a charged non-conducting colloidal spheres [10].

Next comes the method of diffusiophoresis which was first established by Derjaguin [6], and much later by Anderson and Prieve when studying migration of particle in salt solution [7]. As a theoretical point of view, the diffusiophoresis mechanism is the motion of particle caused by a concentration gradient of molecular substances which is due to the formation of the absorption layer of neutral solutes or ions at the surface of the particle [8].

By comparison to electrophoresis and diffusiophoresis, the physical properties of thermophoresis were developed much later by scientists as Ruckenstein when dealing with thermophoresis for colloidal particles [11], by Giddings [12], Brochard and de Gennes when studying the effect of hydrodynamic interactions in thermophoresis for polymer [25]. Thermophoresis is the movement of particle driven by a temperature gradient. For charged particles, the basis of this transport mechanism is the formation of the electric double-layer or the absorption layer around the dissolved particles.

1.3 Motion in a temperature gradient

Thermophoresis mechanism is strongly based on the phenomenon of thermo-osmosis which is defined as a flow of a charged liquid driven by a temperature gradient [8]. The origin of thermo-osmosis was first discussed theoretically and experimentally

by Derjaguin and Sidorenkov [14]. Indeed, thermo-osmosis is due to the response of co-ions and counterions present in the interfacial region to the applied or generated temperature gradient. The thermo-osmotic mechanism can be explained in two ways: First, the strong presence of excess ions in the interfacial region leads to an excess pressure within the diffuse region. Second, the presence of a temperature gradient causes the motion of ion-species to the hot or the cold region. This motion of ions leads to a variation of the pressure within the interfacial region, which is higher at the cold region and lower at the hot region. As a consequence, there is a flow of a charged fluid toward higher pressure to lower pressure. Due to this flow of ions, the particle moves in opposite direction to the temperature gradient. The particle velocity is directly proportional to the temperature gradient where the constant of proportionality is the thermophoretic mobility D_T .

However, the question of which direction the particle moves was not clear. When calculating the thermophoretic coefficient of a colloidal particle in an electrolyte solution, Ruckenstein provided a first answer by stating that a particle always moves towards the cold region [11]. Recent experiments studying mechanism of hot colloids in electrolyte solution, however, showed that particles can move in either direction. Among these experiments, one can cite the work reported by Simoncelli *et al.* [15]. They have trapped optically a Janus particle in a focused laser beam and have measured the vertical position of particle in 10mM of ionic strength in function of the increasing laser power. The important observation is when they used different electrolytes NaCl, NaOH, and LiCl, then the behavior of the particle significantly changes. Another experiment by Eslahian *et al.* reports a rather similar behavior [16]. Here, they have measured the particle's velocity in a mixed electrolyte solution $\text{NaOH}_x\text{Cl}_{1-x}$ in function of a parameter x . When this parameter x varies from 0 to 1, the electrolyte solution changes gradually from NaCl to NaOH, and, as the result, the sign of the particle's velocity becomes positive or negative, respectively. This change of sign of the particle's velocity is generally due to the thermal induced salt-gradient and eventually to the electrolyte Seebeck effect [17, 18, 19]: An applied temperature gradient exerts thermal forces on salt-ions, which depending on their solvation enthalpy, move to the hot or the cold boundaries. As a consequence, this motion of ions leads to the existence of an electric field known as Seebeck field. This generated Seebeck field is due to the motion of salt-ions once a temperature gradient is present in an electrolyte solution, and plays a very important role because it gives a new contribution on the particle's velocity, which is similar to Smoluchowski's electrophoretic mobility

[1]. In more general cases, this Seebeck effect can also determines the direction of motion of particle.

1.4 Summary

The aim of this present work is to study the thermophoresis mechanism for hot colloid particle immersed in an electrolyte solution, and for polyelectrolytes. For colloid particle, the self-propulsion mechanism is largely induced by the electrolyte Seebeck effect which in turn results from the existence of the temperature gradient in the system. In the case of a metal capped colloid, the system generates an dipolar electric field which acts on the electric double-layer and self-propels the particle by thermo-electrophoresis. The resulting particle velocity is directly proportional to the applied thermal gradient and the constant of proportionality is known as a thermophoretic mobility. This mobility depends upon on several parameters like the electrolyte Seebeck coefficient, the solvent salinity and the particle size. For polyelectrolytes, the thermophoresis mechanism arises from the hydrodynamic interactions between the repeat units in the polymer chain. In other words, the transport mechanism is induced by the two dominant forces which are the thermally induced permittivity gradient and the electrolyte Seebeck effect.

This thesis is organized as follows: In section 2, we review previous results on the electrolyte Seebeck effect. In section 3, we theoretically study the Seebeck effect of a heated Janus colloid immersed in an electrolyte solution. We will try to see how the self-propulsion mechanism induced by thermoelectric field can depend on the surface properties of the particle. This particle's surface can be in a different geometries where the system is in non-equilibrium condition and the resulting electric properties is treated within the Poisson-Boltzmann theory. In the case of an conducting surface, the particle carry a high electrical conductivity on its metal cap which forms an isopotential surface. This isopotential condition imposes a significant polarization charge which modifies the double-layer potential and the thermoelectric properties. In section 4, we will discuss about the effect of hydrodynamic interactions in a dilute polyelectrolyte solution. This last point was studied in term of series expansion for Oseen tensor. In addition, we will see, in this section, how the counterions condensation effect can play an essential role on the thermophoretic mechanism for DNA. Finally in section 5, we will study the dynamics of ion, in electrolyte solution, depending on time. Here, the system is in non-stationary state. In this case, the characteristic time scale for ions diffusion

will results from the charge conservation equation which rely the ionic current and the electric charge density.

Chapter 2

Electrolyte Seebeck effect

In this chapter, we review known results on the electrolyte Seebeck effect in different geometries. All the following results in this part are taken from the paper in Ref. [29]

2.1 Seebeck effect in a 1-D geometry

In electrolyte solution, an applied temperature gradient exerts thermal forces on salt-ions which migrate along the gradient. By response, the system generates a macroscopic thermoelectric field which in the one-dimensional system, is given by

$$\mathbf{E} = S \nabla T (1 - e^{-z/\lambda}), \quad (2.1)$$

where S is a constant of proportionality between the electric field E and the temperature gradient, λ the thickness of the electric double-layer and z the normal coordinate perpendicular to the screened surface. The coefficient S is known as an electrolyte Seebeck coefficient [30, 31]. In the one-dimensional case, the temperature gradient present in the system is constant. So if we define T_2 as the temperature of the hot boundary and T_1 the temperature of the cold boundary, then the temperature gradient reads,

$$\nabla T = \frac{T_2 - T_1}{L},$$

where L is the length of the system.

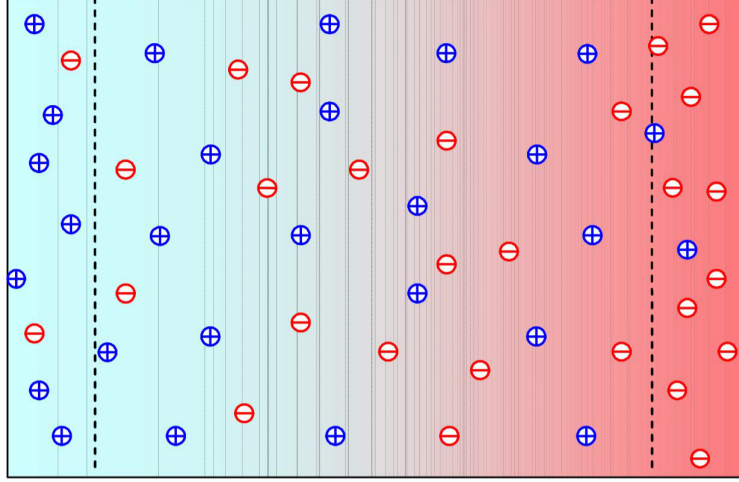


Figure 2.1: Schematic view of the Seebeck effect in a 1 dimensional system. Due to the presence of a temperature gradient, cations and anions accumulate at the cold and hot boundaries, respectively. This result in the macroscopic thermoelectric field $\mathbf{E} = S\nabla T$ which is constant in the bulk and vanishes at the boundaries. This figure is reprinted with permission from Ref. [29].

The physical process of the generation of the electrolyte Seebeck field is sketched in Fig. 2.1 with positive and negative ions located in the cold and hot region, respectively. The motion of ions generates a current which in turn break the uniformity of the electrolyte solution. We will show in next section that this current for positive and negative ions is different because it depends on their heat of transport and the reduced Soret coefficient. Once a charge separation appears between the two boundaries, then the system generates a thermoelectric field which in turn acts on the ions and drives them. The behavior of this thermoelectric field is well described by Eq. (2.1) where the exponential factor describes the accumulation of charges in the hot and cold boundaries. In the bulk, the thermoelectric field takes the expression $\mathbf{E} = S\nabla T$ which is constant in volume, whereas it vanishes at the boundaries. In addition, the sign and magnitude of the Seebeck field depends on the coefficient S which can be positive or negative depending on the solution used.

The corresponding thermocharge density follows from Gauss's law, $\rho = \varepsilon \operatorname{div} E$, and its expression reads as,

$$\rho = -\frac{\sigma}{\lambda} e^{-z/\lambda},$$

where $\sigma = \pm \varepsilon S \nabla T$ takes opposite signs at the cold and hot boundaries. In the bulk, the thermocharge density vanishes, $\rho = 0$, and in the boundaries it's screened by counterions.

2.2 Seebeck effect in 3-D system

Here we detailed the Seebeck effect in the vicinity of a heated colloidal particle. In the system, the particle, totally covered by a thin metal layer, generates a temperature gradient once heated. As illustrated in Fig. 2.2, due to the presence of this temperature gradient, the co-ions move to the hot region (near the particle surface) whereas the counterions move to the cold region. This phenomenon of charge separation induces a thermoelectric field which at distances well beyond the Debye length reads as $\mathbf{E} = S \nabla T$. Thus, near the particle surface the complete expression of the Seebeck field come from the stationary electro-osmotic equation for the ionic current.

2.2.1 ion current

The colloid particle is immersed in an electrolyte solution composed of monovalent ions with densities n_{\pm} for respectively positive and negative ions. Once the particle is heated, it generates a symmetric temperature gradient. This temperature gradient exerts thermal forces on salt-ions and induces their motions. As a result, the system generates an ionic current

$$\mathbf{J}_{\pm} = -D_{\pm} \left(\nabla n_{\pm} + 2n_{\pm} \alpha_{\pm} \frac{\nabla T}{T} \mp n_{\pm} \frac{e \mathbf{E}}{k_B T} \right), \quad (2.2)$$

where D_{\pm} the positive and negative ionic diffusion coefficient. The vector field \mathbf{J}_{\pm} is the current of positive and negative ions. This current is the sum of three different terms: the diffusion current $\propto \nabla n_{\pm}$ which is given by Fick's law, the thermodiffusion current $\sim \alpha_{\pm} \nabla T$ with α_{\pm} the reduced Soret coefficient which characterize the drift of ions in presence of the temperature gradient, and the electric driven current $\propto \mathbf{E}$ which is due to the presence of the thermoelectric field in the system. When the system reaches the steady-state, the three different currents, which are the diffusion currents cancel each other, resulting in $\mathbf{J}_{\pm} = 0$.

In the following, we will detail the behavior of the thermoelectric field and the total charge density in the steady state where the mobile ionic current given by each ionic species vanishes.

2.2.2 Thermoelectric field and thermocharge

Here we give the complete expression of the thermoelectric field of a uniform particle of radius a and centered at $\mathbf{r} = 0$. We denote by n_0 the bulk salinity and $\rho = e(n_+ - n_-)$ the charge density. If we assume that ion densities n_{\pm} differ only weakly from their bulk value, that is $n_+ + n_- \approx 2n_0$ and $\rho/e \ll n_0$, one can linearize the sum of $J_+ - J_-$ in the following form,

$$\nabla\rho + 2n_0e(\alpha_+ - \alpha_-)\frac{\nabla T}{T} - 2n_0e^2\frac{\mathbf{E}}{k_B T} = 0. \quad (2.3)$$

Thus we can perform Eq. (2.3) by applying the relation between the thermoelectric field E and charge density ρ , called Gauss's law

$$\nabla\mathbf{E} = \rho/\varepsilon, \quad (2.4)$$

where ε the solvent permittivity. Inserting this last equation into Eq. (2.3) in the steady state, one obtains the equation satisfied by the thermoelectric field,

$$\nabla^2\mathbf{E} - \frac{1}{\lambda^2}(\mathbf{E} - S\nabla T) = 0, \quad (2.5)$$

where $\lambda^2 = \epsilon k_B T / 2n_0 e^2$ is the Debye screening length and $S = (\alpha_+ - \alpha_-) k_B / e$ is the Seebeck coefficient. The vector quantities \mathbf{E} , ∇T in Eq. (2.5) are considered to be symmetric in the case of an isotropic surface (uniform colloid particle). Now if we consider a 3-D spherical symmetry, only their radial components are finite, i.e, they depend only on the radial distance r from the particle center.

The temperature gradient remains always in the stationary state because of the fact that heat diffuses much faster than ions, and its expression is given by

$$\nabla T = -\frac{\delta T a}{r^2},$$

where δT is the excess temperature at the particle surface. To solve Eq. (2.5), one has to specify the boundary conditions. Here the particle is considered to be

uncharged, i.e, it doesn't carry surface charge. In this case, the thermoelectric field is equal zero at the particle surface, $E(r = a) = 0$. The second condition states that the thermoelectric field vanishes at large distances, $E \rightarrow 0$ when $r \rightarrow \infty$.

With these two conditions and solving Eq. (2.5), the thermoelectric field reads as,

$$E = S \nabla T \left(1 - \frac{r + \lambda}{a + \lambda} e^{(a-r)/\lambda} \right). \quad (2.6)$$

This last equation characterizes the behavior of the thermoelectric field in the vicinity of a heated gold colloid particle. This Seebeck field takes its origin from the separation of charges caused by the temperature gradient. In addition, it's important to note that this thermoelectric field is not an external applied field but the field generated by the system composed of colloid particle plus electrolyte solution.

In the steady-state, the thermoelectric field present in the solution is described by Eq. (2.6), where at distance well beyond $(a + \lambda)$ the screening exponential term vanishes and the remainder long-range electric field $E = S \nabla T$ varies with the inverse of the square distance. Applying Gauss'law, the thermocharge density will scale as, $\rho \propto e^{(a-r)/\lambda}$, which vanishes at long distances well beyond the Debye screening length.

The total thermocharge is found by integrating the thermocharge density over the particle surface, then it reads as

$$Q = -e \widehat{S} \frac{a}{l_B} \frac{\delta T}{T}, \quad (2.7)$$

where \widehat{S} the reduced Seebeck coefficient. This is the net thermocharge accumulated in the vicinity of the particle surface. The thermocharge Q is independent of the radial distance r and thus its sign depends on the coefficient \widehat{S} which is positive for NaCl solution and negative for NaOH solution [32]. The sign of the thermocharge Q tells which ion species is accumulated in the particle's vicinity. For example, in NaCl solution, anions diffuse toward high temperature thus negative charge is accumulated at the particle surface, resulting in $Q < 0$; whereas for NaOH solution, the inverse phenomenon occurs and the particle accumulated a net positive charge. For typical value of the excess temperature $\delta T = 30\text{K}$ and a particle size about $a \sim 1\mu\text{m}$ in NaCl or NaOH electrolyte solution, the corresponding net thermocharge is about $Q \sim 100e$. For protonated salts in water or alcohol solution, the value of the thermocharge becomes much higher.

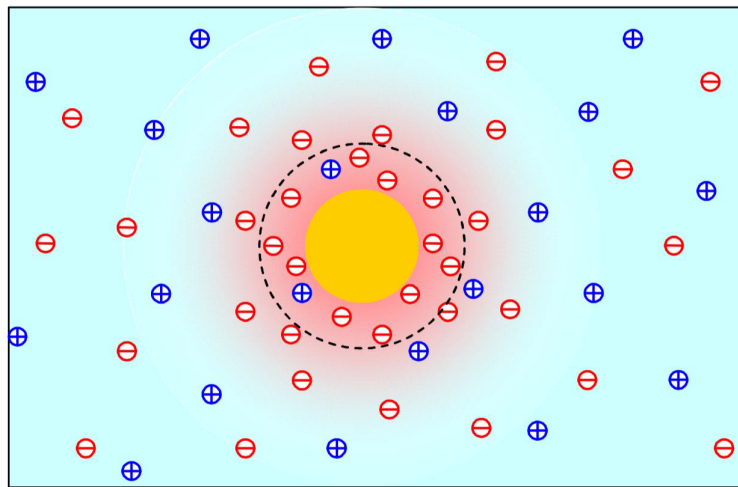


Figure 2.2: Schematic view of the Seebeck effect in a 3 dimensional system. We show here the Seebeck effect in the vicinity of a hot colloid particle. Due to the thermal gradient, the particle accumulates a net thermocharge Q and thus results in a radial thermoelectric field given in Eq. (2.6). This figure is reprinted with permission from Ref. [29].

Chapter 3

Nanoscale Seebeck effect

3.1 Introduction

In recent years, artificial microswimmers have attracted much attention in many different areas such as microfluidic application [21]. In some physical systems, the motion of particles is due to an external applied field like a uniform electric field (electrophoresis) or a chemical (diffusiophoresis) or temperature gradient (thermophoresis). If phoretic motion of passive particles is rather well understood [1, 22, 18], this is not always the case for self-propelled particles. In these systems, it's more difficult to predict the direction of motion of particle or to describe exactly all the physical forces inducing the motion of particle.

Recent experiments on half-metal coated colloid particles (Janus particle), in a defocused laser beam [38] or by optical trapping [39], reveal the strong presence of thermophoresis forces in the sense that: Once the particle is heated, the absorption of laser by the metal side generates a local temperature gradient which in turn drives the particle by thermophoresis. To go even further in to order understand more the question of self-propulsion mechanism induced by thermophoresis, the colloids particles are immersed in electrolyte aqueous solution. In this situation, recent experiment reveals that the stationary height of colloid particle increases with the laser power, and even varies with the ion species [15]. In other words, this last point means the sign and magnitude of thermophoresis depend strongly on the electrolyte composition; this was confirmed by recent work on hot colloids [16]. In addition to thermal effect, one observes thermoelectric effect, called electrolyte Seebeck effect, which occurs during the self-propulsion mechanism of hot colloid

particle in an electrolyte solution. This Seebeck effect plays an essential role on the transport mechanism of hot particle, and even depends on the surface properties of the particle. It's important to question that how the thermoelectric properties with the induced slip-velocity v_s can change at an insulating and conducting surfaces.

In this present chapter, we deal with the self-propulsion mechanism of hot Janus colloid induced by thermoelectrophoresis: As illustrated in Fig. 3.1, due to the presence of a temperature gradient, the Janus particle, immersed in a electrolyte solution, carries opposite thermocharges on its two poles which in turn results in a dipolar thermoelectric field. This field acts on the electric double-layer and self-propels the particle with velocity u . The transport velocity can be derived directly when taking the surface configurational average of the boundary slip-velocity v_s which is a function of the parallel thermoelectric field $E_{\parallel} = S\nabla_{\parallel}T$. This parallel field is modified close to a conducting surface but does not change at an insulating surface (upper and lower hemispheres in Fig. 3.1c). At the conducting surface, the gold cap forms an isopotential surface because of its high electrical conductivity, thus the parallel electric field vanishes. In both cases, the resulting transport velocity does not be changed by the surface electric properties, but in turn depends strongly on the salt composition.

3.2 Boundary layer approximation

3.2.1 Electrostatic boundary conditions

Surface charges of colloidal particles are usually treated in Poisson-Boltzmann theory. Since an analytic solution exists in one dimension only, the widely used boundary layer approximation neglects the surface curvature. As long as the screening length λ is much smaller than the particle radius a , there is a separation of length scales: The properties of the electric double layer vary much more rapidly in perpendicular direction than parallel to the surface.

The resulting approximation is best discussed in terms of Gauss' law $\rho = \text{div}(\varepsilon\mathbf{E})$. This divergency comprises two terms, the normal field component decays on the scale of the Debye length, $\partial_z E_{\perp} \sim E_{\perp}/\lambda$, whereas the permittivity and the parallel electric field vary on the scale of the particle radius, $\partial_x E_{\parallel} \sim E_{\parallel}/a$. Thus to linear order in small parameter λ/a , the divergency of the electric field is given

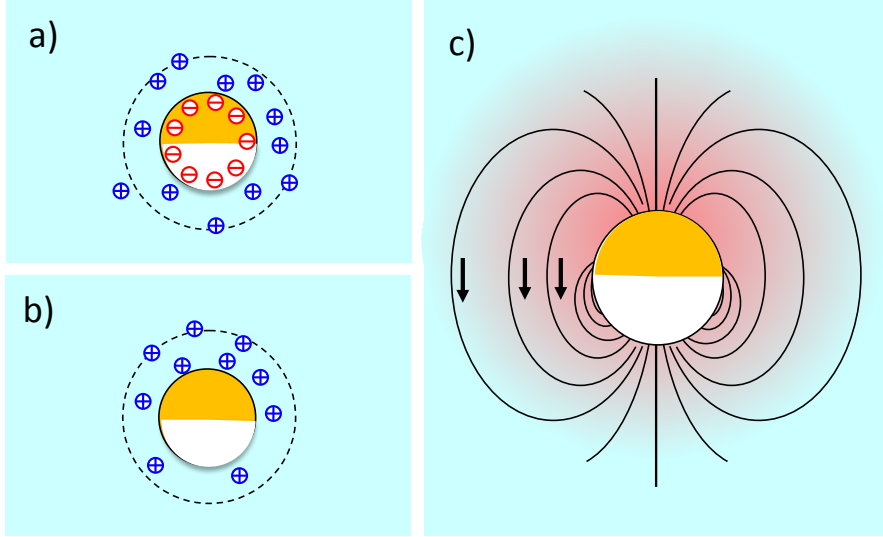


Figure 3.1: Schematic view of a thermoelectric self-propulsion mechanism of a heated Janus particle. a) The electric double-layer of a charged Janus particle immersed in an electrolyte solution. The ions are screened with a valency of the order of $z \sim 10^5$. The Debye length λ , characterizing the thickness of the electric double-layer (dashed line), is much smaller than the particle radius $a \sim 1 \mu\text{m}$. b) Thermocharge accumulated by the electrolyte Seebeck effect ($S < 0$); the resulting (positive and negative) thermocharge density is larger at the hot metal cap; for an excess temperature of a few kelvin one has a net charge of about $Q_T \sim 100e$ [40]. c) Dipole component of the thermoelectric field \mathbf{E} in the vicinity of a heated Janus particle. The parallel field E_{\parallel} vanishes at the metal cap (upper hemisphere), but is finite at the insulating surface.

by its normal coordinates,

$$\frac{dE_{\perp}}{dz} = \frac{\rho}{\varepsilon}. \quad (3.1)$$

For further use, we integrate from the surface to a distance B that is much larger than the screening length but much smaller than the particle radius, and find

$$E_{\perp}(B) - E_{\perp}(0) = \frac{1}{\varepsilon} \int_0^B dz \rho(z) \equiv \frac{\sigma}{\varepsilon}. \quad (3.2)$$

The second identity defines the charge density per unit area of the diffuse layer. This parameter also determines the double-layer potential φ_{σ} , as is obvious from the Poisson-Boltzmann mean-field expression for the diffuse layer, $\rho = 2en \sinh(e\varphi_{\sigma}/k_B T)$.

In the case of an electric double layer at equilibrium, the electric field usually vanishes at large distance, $E_{\perp}(B) = 0$, resulting in the value at the particle surface

$$E_{\perp}(0) = -\frac{\sigma}{\varepsilon}. \quad (3.3)$$

Then $-\sigma$ corresponds to the charge per unit area of the surface, which exactly cancels that of the diffuse layer.

On the contrary, the main results of the present paper are derived from Eq. (3.2), with the outer boundary condition determined by $E_{\perp}(B) = S\nabla_{\perp}T$. This implies that σ as defined in (3.2) does not correspond to the surface charge density. In the range of the distance B , the temperature gradient is almost identical to that at the particle surface, $\nabla_{\perp}T = \nabla_{\perp}T_S$.

3.2.2 Temperature gradient at the particle surface

Since the heat conductivities of liquid and solid are different in general, the particle deforms the temperature field in its vicinity. For a sphere, a conductivity contrast modifies the parallel and perpendicular components of the temperature gradient according to

$$\nabla_{\parallel}T_S \rightarrow \xi_{\parallel}\nabla_{\parallel}T_S, \quad \nabla_{\perp}T_S \rightarrow \xi_{\perp}\nabla_{\perp}T_S, \quad (3.4)$$

with the well-known constants [32]

$$\xi_{\parallel} = \frac{3\kappa_w}{2\kappa_w + \kappa_P}, \quad \xi_{\perp} = \frac{3\kappa_P}{2\kappa_w + \kappa_P}, \quad (3.5)$$

expressed in terms of the thermal conductivities κ_w and κ_P for the liquid and the solid, respectively. We suppress these factors in the following sections but restore them when discussing the slip velocity.

3.3 Seebeck effect: uncharged particle

Here we evaluate the thermoelectric properties at the particle surface which does not carry a surface charge, i.e, the particle is considered to be uncharged.

3.3.1 Debye-Hückel approximation

Here we derive the thermocharge of an otherwise uncharged hot Janus particle in the weak-coupling approximation where the electrostatic energy $e\varphi$ is much smaller than the thermal one $k_B T$. We start by giving the equation satisfying by the electric field \mathbf{E} and charge density ρ which obtained by using Debye-Hückel approximation,

$$\nabla\rho + \frac{\varepsilon}{\lambda^2}(S\nabla T - \mathbf{E}) = 0. \quad (3.6)$$

This last equation has two unknowns: The thermocharge density ρ and the electric field E . To have only one unknown and simple computations, we solve the corresponding equation satisfying by the electrostatic potential φ . Now introducing the Gauss's law $\rho = \varepsilon \operatorname{div} \mathbf{E}$ with the relation $\mathbf{E} = -\nabla\varphi$ into Eq. (3.6), one has to solve

$$\nabla^2\varphi - \frac{1}{\lambda^2}(\varphi - S\Delta T) = 0, \quad (3.7)$$

where $\Delta T = T(\mathbf{r}) - T_0$ with $T(\mathbf{r})$ the temperature field given in term of a series multipolar expansion and T_0 the bulk temperature (see Appendix A2).

The linear differential equation (3.7) is obtained within the weak-coupling approximation, and his general solution reads as,

$$\varphi = - \sum_{n=0}^{\infty} \left(St_n \frac{a^{n+1}}{r^{n+1}} + c_n \frac{k_n(r/\lambda)}{k_n(a/\lambda)} \right) P_n(c), \quad (3.8)$$

where $c = \cos\theta$ cosine of the polar angle, and $k_n(x) = \sqrt{\frac{2}{\pi x}} K_{n+1/2}(x)$ the modified spherical Bessel function of the second kind.

The potential in (3.8) is still not complete because of the unknown coefficients c_n which can be found by specifying the electrostatic boundary conditions which in turn will depend on the surface properties of the particle. In the following sections, we will try to find the coefficients c_n and discuss the thermoelectric properties for both insulating and conducting surfaces.

3.3.2 Insulating particle

Here the particle does not carry a surface charge, thus the electrostatic boundary conditions require that the normal electric field vanishes at the particle surface, $E_{\perp}(0) = 0$, whereas at the outer boundary one has $E_{\perp}(B) = S\nabla_{\perp}T_S$. From Gauss' law (3.2), one readily finds

$$\varepsilon S\nabla_{\perp}T_S = \int_0^B dz \rho_T(z) \equiv \sigma_T, \quad (3.9)$$

where the second equality defines the thermocharge per unit area. As illustrated in Fig. 3.1b, a negative Seebeck coefficient implies a positive surface charge at the hot boundary, $\sigma_T > 0$. In general, the temperature varies along the particle surface, and so does $\sigma_T = \sigma_T(x)$.

With the boundary conditions in (3.9), the electrostatic potential completely reads as

$$\varphi = -S \sum_n t_n P_n(c) \left(\frac{a^{n+1}}{r^{n+1}} - (n+1) \frac{\lambda}{r} e^{(a-r)/\lambda} \right). \quad (3.10)$$

Before computing the component of the electric field, we approximate that, within the screening layer, the factor $(a/r)^n$ is close to unity, thus we discarded the corresponding factor in the following equations. Applying this last approximation and taking the perpendicular derivative of the potential φ , the normal component of the electric field reads, to leading order in λ/a ,

$$E_{\perp} = S\nabla_{\perp}T(1 - e^{-z/\lambda}), \quad (3.11)$$

where $\nabla_{\perp}T \approx (T_S - T_0)/a$ with T_S the temperature field at the particle surface.

The normal component of the electric field is screened by the thermocharge such that it vanishes at the surface. The parallel component, on the other hand, remains unchanged and is finite at the surface,

$$E_{\parallel} = S\nabla_{\parallel}T_S, \quad (3.12)$$

where the parallel gradient of the temperature field is taken to be $\nabla_{\parallel}T_S \approx \sin \theta \delta T/a$.

The thermocharge density follows from Gauss' law, $\rho_T = -\nabla^2\varphi$. With the same approximation as for the normal field component above, one finds for the thermocharge density

$$\rho_T = -\frac{\sigma_T}{\lambda} e^{-z/\lambda}, \quad (3.13)$$

with $\sigma_T = \varepsilon S \nabla_{\perp} T_S$ the thermocharge per unit area.

This thermocharge density ρ_T decreases exponentially before it vanishes at large distances well beyond the Debye screening length. Since the Debye screening length λ is much smaller than the particle radius a , then the temperature gradient $\nabla_{\perp} T$ is taken to be constant through the charged layer. For a micron size particle at an excess temperature of 10 K, and a typical Seebeck parameter $S = 10^{-4}$ V/K, the surface charge density σ_T takes a value of about $10e$ per square micron and the electric field about 1 kV/m.

3.4 Charged surfaces

3.4.1 Poisson- Boltzmann theory

In the previous sections, we derived and discussed about the thermoelectric properties for a hot colloid particle in the Debye-Hückel approximation where the electrostatic energy $e\varphi$ is much smaller compared to the thermal energy $k_B T$. In the case of a strong charged particle, this last point is necessary satisfied because of strong-coupling system and the electrostatic properties will be governed by the well-known Poisson-Boltzmann equation.

Contrary to Debye-Hückel approximation, where all the derived equations are linear, the Poisson-Boltzmann equation is non-linear and does not have an analytical solution in a 3D system. To overcome this difficulty, we resort to the usual boundary layer approximation: The particle radius is much larger than the Debye screening length, $a \gg \lambda$. As a consequences, the particle surface can be considered as flat and the resulting non-linear Poisson-Boltzmann equation will be treated in planar geometry where the solution results in a 1D problem.

Consider a hot charged particle with a surface charge σ in contact with electrolyte solution. Within the above approximation, the electrostatic potential satisfy the 1D equation,

$$\partial_z^2 \varphi_{\sigma} = \frac{k_B T}{e \lambda^2} \sinh \frac{e \varphi_{\sigma}}{k_B T}, \quad (3.14)$$

where z is the normal distance to the particle surface. The solution of this equation is well-known and results in,

$$\varphi_{\sigma}(z) = -\frac{2k_B T}{e} \ln \frac{1 + g e^{-z/\lambda}}{1 - g e^{-z/\lambda}}, \quad (3.15)$$

with the shorthand notation

$$\hat{g} = ge^{-z/\lambda}, \quad g = \sqrt{1 + \ell^2/\lambda^2} - \ell/\lambda.$$

The parameter g is given by the ratio of the Gouy-Chapman length ℓ and the Debye length λ ,

$$\ell = \frac{e}{2\pi\ell_B|\sigma|}, \quad \lambda = \frac{1}{\sqrt{8\pi\ell_B n}},$$

where the Bjerrum length ℓ_B , the surface charge density σ , and the salinity n . In the following we assume a negative surface charge $-\sigma$.

Taking the perpendicular derivative $d\varphi/dz$, the normal electric field reads

$$E_{\perp} = -\frac{\sigma}{\varepsilon}e^{-z/\lambda}\frac{1-g^2}{1-\hat{g}^2}. \quad (3.16)$$

This field is perpendicular to the particle, and it satisfy the relation $E(0) = -\sigma/\varepsilon$.

The charge density in the diffuse layer is readily obtained from Gauss' law $\rho = \varepsilon dE/dz$,

$$\rho = \frac{\sigma}{\lambda}e^{-z/\lambda}\frac{(1-g^2)(1+\hat{g}^2)}{1-\hat{g}^2}. \quad (3.17)$$

Integrating over z one finds

$$\int_0^{\infty} dz\rho(z) = \sigma, \quad (3.18)$$

which means that the counterions ρ completely screen the surface charge density $-\sigma$.

We briefly reviewed the Poisson-Boltzmann theory in thermal equilibrium, then we will discuss in the following sections about thermoelectric properties for both insulating and conducting surfaces.

3.4.2 Charged insulating surface

Now we consider an insulating surface with an electric double layer. In this case, the diffuse layer consists of both double-layer and thermocharge contributions,

$$\rho = \rho_0 + \rho_T. \quad (3.19)$$

For notational convenience we assume a negative surface charge density $-\sigma_0$, as is the case for most colloids. Then the electric field at the outer boundary is given by the Seebeck field, and at the inner one by $E_{\perp}(0) = -\sigma_0/\varepsilon$, and Eq. (3.2) becomes

$$S\nabla_{\perp}T_S + \frac{\sigma_0}{\varepsilon} = \frac{1}{\varepsilon} \int_0^B dz(\rho_T + \rho_0) = \frac{\sigma_I}{\varepsilon}, \quad (3.20)$$

with the charge density of mobile ions per unit area,

$$\sigma_I = \sigma_T + \sigma_0. \quad (3.21)$$

Note that the two contributions are related to the Seebeck field and to the surface charge, respectively.

The corresponding Poisson-Boltzmann potential φ_{σ_I} , which is defined through $\rho_T + \rho_0 = \varepsilon \partial_z^2 \varphi_{\sigma_I}$, has to be calculated with an effective surface charge $\sigma_I = \sigma_T + \sigma_0$, with the parameter

$$g = \sqrt{1 + l^2/\lambda^2} - l/\lambda,$$

where the Gouy-Chapman length,

$$l = \frac{e}{2\pi l_B |\sigma_0 + \varepsilon S \nabla_{\perp} T_S|}. \quad (3.22)$$

Taking the normal derivative of the total electrostatic potential, $\varphi_I = \varphi_T + \varphi_{\sigma_I}$, the normal component of the electric field reads

$$E_{\perp}^{\text{ins}}(z) = S\nabla_{\perp}T - \left(\frac{\sigma_0}{\varepsilon} + S\nabla_{\perp}T \right) e^{-z/\lambda} \frac{1 - g^2}{1 - \hat{g}^2}. \quad (3.23)$$

The second term of this last equation result from the perpendicular derivative of φ_{σ_I} , and it decays rapidly through the screening layer. Because of the constant temperature gradient $\nabla_{\perp}T$ through the charged layer, the first term is constant on the scale of the Debye length. One readily verifies that $E_{\perp}(z)$ satisfies the boundary condition, at the particle surface $E_{\perp}(0) = -\sigma_0/\varepsilon$, and well beyond the screening length $E_{\perp}(B) = S\nabla_{\perp}T$.

The parallel component of the electric field reads as,

$$E_{\parallel}^{\text{ins}}(z) = S\nabla_{\parallel}T - \nabla_{\parallel}\varphi_{\sigma_I}. \quad (3.24)$$

This parallel field does not vanish at the surface $z = 0$ because the second term gives rise to a term proportional to $\propto \nabla_{\parallel}T$. Both contributions vary slowly on the scale of the particle radius and are of comparable magnitude.

3.4.3 Charged conducting surface

Now we turn to conducting surfaces, for example the gold cap of the upper hemisphere in Fig. 3.1c. Because of its high electric and thermal conductivities, the metal layer may considerably modify the thermoelectric properties in the double-layer and at the particle surface. The electrostatic boundary conditions impose a constant potential, or a vanishing parallel electric field [41],

$$E_{\parallel}(0) = S\nabla_{\parallel}T - \nabla_{\parallel}\varphi_{\sigma_C}(0) = 0. \quad (3.25)$$

On the other hand, at the outer boundary $z = B$ the parallel field takes the finite value $\nabla_{\parallel}T$. These conditions cannot be satisfied with the surface charge discussed above.

To achieve (3.25) the mobile electrons in the metal surface move until their polarization charge density σ_P modifies the double-layer potential such that its gradient cancels the thermoelectric field at the surface. In one hand, the polarization charge is determined by inserting φ_{σ} with

$$\sigma_C(x) = \sigma_T(x) + \sigma_0 + \sigma_P(x) \quad (3.26)$$

in Eq. (3.25) and solving for σ_P . In the other hand, we assume that the total charge does not change, so one has for the surface integral $\int dS\sigma_P = 0$. With these two conditions, the polarization charge is determined by

$$\sigma_P = -\sigma_0 \left(\frac{e\sqrt{1+b^2}}{k_B T} (ST - \zeta) - \frac{d \ln \varepsilon}{d \ln T} - 1 \right) \frac{T_S - \langle T_S \rangle}{2T}, \quad (3.27)$$

where T_S the temperature field at the particle surface and $\langle T_S \rangle$ its mean value, $b = l/\lambda$ the ratio of the Gouy-Chapman length and screening length, and ζ the surface potential.

In the weak-coupling limit, the Gouy-Chapman length l is much larger compared to the Debye screening length, $b = l/\lambda \gg 1$. Thus expanding in linear order Eq. (3.27), the polarization charge will be simplified as

$$\sigma_P = -\frac{\varepsilon S}{\lambda} (T_S - \langle T_S \rangle). \quad (3.28)$$

Since the diffuse layer screens the local surface charge density, σ_P induces a corresponding change of the mobile charge density, ρ_P , and we have $\rho_C = \rho_T + \rho_0 +$

ρ_P . We recall that the double-layer potential φ_σ is calculated with the parameter σ_C which accounts for the charge density of the diffuse layer, $\sigma_C = \int dz \rho_C(z)$, whereas the surface charge density is given by $-(\sigma_0 + \sigma_P)$. Accordingly, we have

$$E_\perp(0) = -\frac{\sigma_0 + \sigma_P}{\varepsilon} \quad (3.29)$$

at the particle surface.

Now taking the normal and the parallel derivative of the total potential, $\varphi = \varphi_T + \varphi_{\sigma_C}$, the normal component of the electric field reads as

$$E_\perp^{\text{cond}}(z) = -\left(\frac{\sigma_0 + \sigma_P}{\varepsilon} + S\nabla_\perp T\right) \frac{1 - g^2}{1 - \widehat{g}^2} e^{-z/\lambda} + S\nabla_\perp T, \quad (3.30)$$

for the parallel field component, one has

$$E_\parallel^{\text{cond}}(z) = \left(1 - \frac{1 - g^2}{1 - \widehat{g}^2} e^{-z/\lambda}\right) S\nabla_\parallel T. \quad (3.31)$$

At the particle surface, one can verify that E_\perp^{cond} satisfies Eq. (3.29) whereas for the parallel field is zero at the particle surface $E_\parallel^{\text{cond}}$ vanishes. As shown in Fig. 3.2, with increasing distance, the double-layer potential φ_σ decays and vanishes well beyond the screening length, and the electric field is given by, $\mathbf{E} = S\nabla T$.

3.5 Hydrodynamic phoretic velocity

3.5.1 Slip-velocity

Closely following Ref. [32], we evaluate the boundary slip-velocity v_s which is derived from a fluid mechanical treatment. For that we adopt the low Reynold number hydrodynamic Stokes equation which describes the velocity field of an incompressible fluid ($\nabla \cdot \mathbf{v} = 0$) in the steady state,

$$\eta \nabla^2 \mathbf{v} = \nabla P - \mathbf{f}, \quad (3.32)$$

where η the solvent viscosity, P the osmotic pressure, and \mathbf{f} the force exerted by the particle on the surrounding charged fluid (force per unit volume).

For an approximate solution of the Stokes equation, we consider a geometry where the Debye screening length is much more smaller than the particle radius,

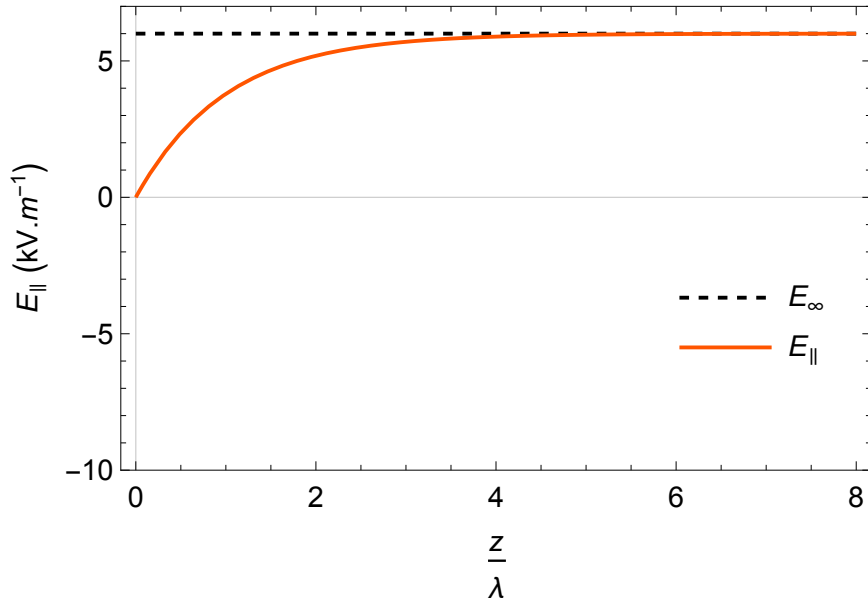


Figure 3.2: Variation of the parallel component $E_{\parallel}^{\text{cond}}$ of the electric field in function of the ratio of the normal distance z and the Debye length λ . For the plot we used the following parameters: The Seebeck coefficient for NaOH solution $S = -200\mu\text{V}/\text{K}$, particle radius $a = 1\mu\text{m}$, the Debye length $\lambda = 30\text{nm}$, and the excess temperature $\delta T = 30\text{K}$. The dashed lines indicate, the long-range thermoelectric field $E_{\infty} = -S\delta T/a \approx 6\text{kV}/\text{m}$.

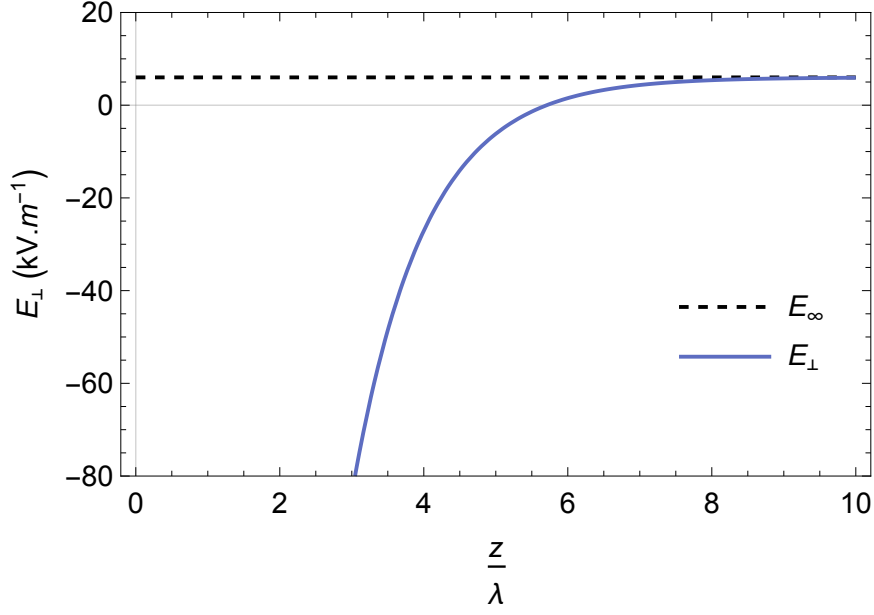


Figure 3.3: Variation of the normal component E_{\perp}^{cond} of the electric field in function of the ratio of the normal distance z and the Debye length λ . For the plot we used the following parameters: The Seebeck coefficient for NaOH solution $S = -200\mu\text{V}/\text{K}$, particle radius $a = 1\mu\text{m}$, the Debye length $\lambda = 30\text{nm}$, and the excess temperature $\delta T = 30\text{K}$. The dashed lines indicate, the long-range thermoelectric field $E_{\infty} = -S\delta T/a \approx 6\text{kV}/\text{m}$, and the normal field at the particle surface $E_{\perp}(z = 0) = -(\sigma_0 + \sigma_P)/\varepsilon \approx -1.8 \times 10^3\text{kV}/\text{m}$.

$\lambda \ll a$. In this case, the particle surface is considered as flat and the hydrodynamics quantities vary slowly along the particle surface, but much more rapidly in the normal direction [1]. Now if we adopt a local coordinates x and z , respectively, parallel and perpendicular to the surface, the normal coordinate of the velocity field vanishes, $v_z = 0$. In the parallel direction, the velocity field depends hardly on the x component, that is $v_x = v_x(z)$, implying the equation $\partial_z^2 v_x = f_x - dP/dx$. Integrating this last equation with the Stokes boundary conditions, where at the surface the velocity vanishes $v_x|_{z=0} = 0$ and becomes constant at a distance equal to the Debye length λ , one finds the boundary slip-velocity as,

$$v_s = \frac{1}{\eta} \int_0^\infty dz z (f_{\parallel} - \nabla_{\parallel} P), \quad (3.33)$$

where η is the solvent viscosity and where the driving force consists of several terms. The first one derives from the Maxwell tensor and contains electric forces,

$$\mathbf{f} = \rho \mathbf{E} - \frac{1}{2} E^2 \nabla \varepsilon, \quad (3.34)$$

that is, the Coulomb force exerted by the electric field on the charge density ρ and the change in electric energy due to a permittivity gradient.

To linear order in the temperature induced perturbations we have

$$\mathbf{f} = \rho_0 (S \nabla T - \nabla \varphi_\sigma) - \frac{1}{2} (\nabla \varphi_{\sigma_0})^2 \nabla \varepsilon, \quad (3.35)$$

where $\nabla \varphi_\sigma$ in the first term still depends on the detail of the electric double layer and, in particular, takes quite a different form at insulating and conducting surfaces.

The second term in (3.33) stems from the pressure $P = \delta n k_B T$ exerted by the excess concentration of mobile ions $\delta n = n [\cosh(e\varphi_\sigma/k_B T) - 1]$ in the double layer. When evaluating the gradient one needs to account for its variation with temperature, salinity, and the potential φ_σ , resulting in

$$\nabla P = -\rho_0 \nabla \varphi_\sigma + (\rho_0 \varphi_{\sigma_0} + \delta n k_B T) \frac{\nabla T}{T} + \delta n k_B T \frac{\nabla n}{n}. \quad (3.36)$$

In these relations for \mathbf{f} and ∇P , the potential φ_σ varies rapidly in normal direction, and slowly along the surface. The quantities T , ε , and n vary slowly in all directions, on the scale of the particle parameter.

Gathering the different terms one obtains the force density

$$\mathbf{f} - \nabla P = \rho_0 S \nabla T - h \frac{\nabla T}{T} - \delta n k_B T \frac{\nabla n}{n} - \frac{1}{2} (\nabla \varphi_{\sigma_0})^2 \nabla \varepsilon, \quad (3.37)$$

where we use the shorthand notation for the double layer enthalpy density $h = \rho_0 \varphi_{\sigma_0} + \delta n k_B T$. As a remarkable feature, the parallel gradient $\nabla_{\parallel} \varphi_{\sigma}$ has disappeared from the double-layer forces. If both the electrostatic force \mathbf{f} and the osmotic pressure P depend on the precise form of the parameter σ , these terms cancel in (3.37). Since $\nabla \varphi_{\sigma}$ is the only term to depend on the polarization charge σ_P , this quantity no longer is relevant and, as a consequence, the slip velocity does not depend on the conductivity of the particle surface.

With the known Poisson-Boltzmann expressions for φ_{σ} and its derivatives, the integral in (3.33) is readily performed

$$v_s = -\frac{\varepsilon \zeta}{\eta} S \xi_{\parallel} \nabla_{\parallel} T + \frac{\varepsilon (\zeta^2 - 3\zeta_T^2) \xi_{\parallel} \nabla_{\parallel} T}{2\eta T} - \frac{\varepsilon \zeta_T^2}{2\eta} \left(\frac{\nabla_{\parallel} \varepsilon}{\varepsilon} + \frac{\nabla_{\parallel} n}{n} \right), \quad (3.38)$$

with the surface potential $\zeta = \varphi_{\sigma_0}(0)$ and the quantity [32],

$$\zeta_T = \left(\frac{2k_B T}{e} \right) \left[\ln \cosh \left(\frac{e\zeta}{4k_B T} \right)^2 \right]^{1/2}. \quad (3.39)$$

For weakly charged surfaces, where the ζ -potential is smaller than $k_B T/e \approx 25$ meV, one has $\zeta_T \approx \zeta$, whereas in the opposite case, ζ_T is significantly smaller than ζ . Note that we have restored the factor ξ_{\parallel} which accounts for the thermal conductivity contrast of particle and solvent.

This result does not depend on the electrical conductivity of the particle surface. The slip velocity is the same at insulating and conducting surfaces, although the electric field at the particle surface shows a very different behavior. A similar effect was shown to occur for the electrophoretic mobility at a metal surface [42], resulting in an electro-osmotic slip velocity that is the same at insulating and conducting surfaces.

3.5.2 Drift velocity

The boundary slip-velocity in (3.38) varies along the particle surface with respect to the polar angle θ . Taking its configurational average along the surface, we find

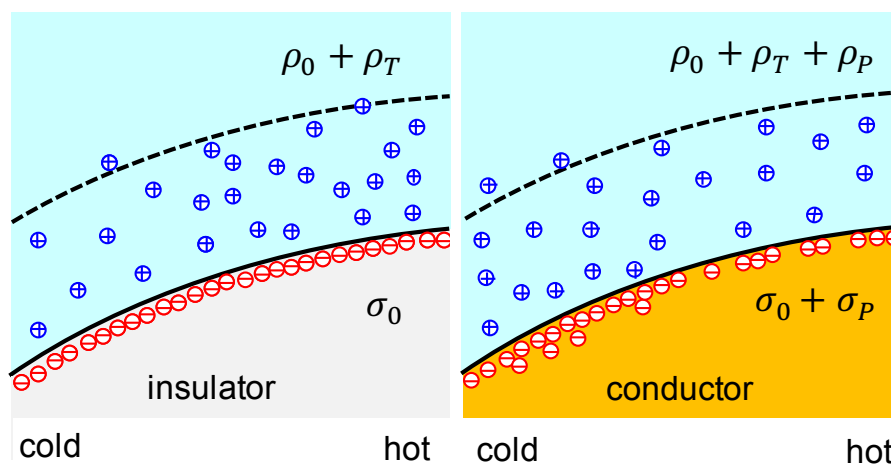


Figure 3.4: Electric double-layer including the thermocharge (temperature increases from left to right). At an insulating surface, the surface charge density σ_0 is not affected by the Seebeck effect, whereas the diffuse layer comprises the non-uniform thermocharge density ρ_T . At a conducting surface (right panel), the condition of a constant surface potential requires a polarization charge σ_P ; the corresponding counterions add to the diffuse layer and to the non-uniform thermocharge.

the particle drift velocity $\mathbf{u} = -\langle \mathbf{v}_s \rangle$ which is opposite to the osmotic flow in the boundary layer. Simplifying the thermal conductivity ratio $\xi_{\parallel} \approx 1$ (particle and solvent thermal conductivities taken to be equal: $k_w \approx k_p$) and taking the surface integral of Eq. (3.38), one readily obtain the particle drift velocity

$$\mathbf{u} = -\frac{\varepsilon(\zeta^2 - \zeta_T^2)}{3\eta} \frac{\nabla T}{T} + \frac{\varepsilon\zeta_T^2}{3\eta} \left(\frac{\nabla\varepsilon}{\varepsilon} + \frac{\nabla n}{n} \right) + \frac{2\varepsilon\zeta}{3\eta} \mathbf{E}_T, \quad (3.40)$$

where the first term results from the thermoosmotic flow in the electric double-layer and the last term accounts for the velocity induced by the self-generated Seebeck field $\mathbf{E}_T = S\nabla T$ with the Helmholtz-Smoluchowski's electrophoretic mobility $\varepsilon\zeta/\eta$ multiplied by the factor 2/3.

As for the slip-velocity, the sign and magnitude of this particle drift velocity does not depend on the electrical conductivity of the particle surface, but vary strongly with the electrolyte Seebeck coefficient S which in turn takes specific values depending on the electrolyte composition used. For NaCl solution, the resulting velocity $\mathbf{u} > 0$, thus the particle moves toward hot region, whereas for NaOH solution, $\mathbf{u} < 0$, one observes the motion of particle in opposite direction.

3.6 Results and discussion

In previous sections, we have already derived the expressions of the electric properties, the thermocharge and the induced transport velocity of an uncharged or charged hot colloid in contact with electrolyte solution. Now we are going to discuss in details about these results, and to see which impact they can have in possible applications.

3.6.1 Thermocharge and electric field

The thermoelectric properties are quite independent of the particle's equilibrium surface charge density. For the sake of clarity, we mainly discuss the case of an uncharged particle.

Due to strong absorption of laser light by the metal cap, the particle generates an asymmetric temperature gradient which in turn creates a thermoelectric field or Seebeck field. This Seebeck field does not result from an externally applied voltage but from the ionic current (2.2) induced by the temperature gradient.

Although the electric boundary conditions at the surface of a dispersed colloidal particle are the same, its behavior in the vicinity are quite different from that of an external electric field, and in particular results in a thermocharge density at the particle surface, which is given by the equation (3.13). The behavior of the thermocharge density does not depend on the surface properties of the particle: In both cases, an insulating and conducting surface, it decays exponentially and takes the value zero at the bulk. Because of the non-uniform temperature gradient along the surface, $\nabla_{\perp}T$ varies slowly along the surface; and with the assumption $\lambda \ll a$, the temperature gradient can be considered as constant through the charged layer. The thermocharge per unit area reads, in the case of a NaOH electrolyte solution carrying an excess temperature of 30K and a Seebeck coefficient $S = -200\mu\text{V/K}$, as

$$\sigma_T = \varepsilon S \nabla_{\perp} T \sim 10^{-4} \text{e/nm}^2. \quad (3.41)$$

In Fig. 3.5, we show the electric field lines around an insulating and conducting particle. We compare first the field lines around the low-permittivity insulating particle shown in Fig 3.4 a and b, then we see secondly the case of an conducting particle. Because of the strong permittivity contrast, when an external electric voltage is applied then the resulting field does not penetrates in the particle. As a consequence, the field at the particle surface is by the factor $3\varepsilon_w / (2\varepsilon_w + \varepsilon_P) \approx 3/2$ greater than in the bulk. On the contrary, the Seebeck field, determined by Eq. (3.6), is not deformed by the permittivity contrast ($\varepsilon_P \ll \varepsilon_w$) in the vicinity of the particle, and everywhere follows the temperature gradient. The explanation of this effect is the fact that the temperature gradient is assumed to be constant everywhere, and the normal component of the thermoelectric field is screened by the accumulation of mobile ions in the vicinity of the particle. On the conducting surface, the polarization effect modifies the double-layer potential and imposes isopotential condition at the metal surface. As a consequences, the parallel field vanishes at the particle surface, and, as illustrated in Fig 3.5c, the thermoelectric field at the particle surface is given by its normal component.

3.6.2 Polarization charge on the conducting surface

We discussed in the section above the thermocharge which occurs on both insulating and conducting surfaces. On the latter, however, the isopotential condition of electrostatics imposes in addition a polarization charge on the metal coating, which is screened by mobile ions. In other words, the thermal polarization effect

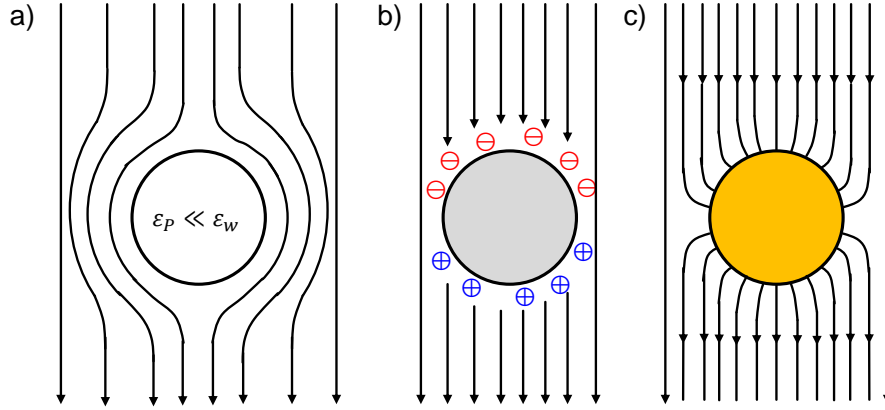


Figure 3.5: Electric field lines for insulating and conducting particles. a) Electric field due to an applied external voltage. The field does not penetrate in a low-permittivity particle, resulting in parallel component at the surface which is by a factor $3\varepsilon_w/(2\varepsilon_w + \varepsilon_P) \approx \frac{3}{2}$ larger than the bulk field. b) Thermoelectric field in the vicinity of an insulating particle. Assuming a constant temperature gradient, that is, similar thermal conductivities of particle and solvent, we find that the field is not deformed by the permittivity contrast ($\varepsilon_P \ll \varepsilon_w$) but follows the constant temperature gradient, $E = S\nabla T$. Within one Debye layer from the particle surface, its normal component E_\perp is screened by ion accumulation, that is, the thermocharge ρ_T , as shown in the left panel of Fig. 3.4; the parallel component E_\parallel does not vanish, and the particle surface is not at constant potential. c) Thermoelectric field in the vicinity of a conducting particle. Polarization of the metal surface adjusts the surface charge density such that the parallel component of the field vanishes, resulting in an isopotential surface. The corresponding non-uniform surface charge σ is illustrated in the right panel of Fig. 3.4. The normal component of the electric field corresponds to the surface charge parameter σ .

modifies the charge parameter σ on the electric double-layer by σ_P which, in the weak-coupling approximation, is given by (3.28).

For a micron size particle in NaOH solution with an excess temperature of 30K, an electrolyte Seebeck coefficient $S = -200\mu\text{V}/\text{K}$ and a Debye length $\lambda = 2\text{nm}$, the polarization charge is of the order of

$$\sigma_P = \frac{\varepsilon S (T_S - \langle T_S \rangle)}{\lambda} \sim 10^{-2} \frac{\text{e}}{\text{nm}^2}. \quad (3.42)$$

From comparison of $\nabla_{\perp} T \approx (T_S - T_0)/a$, it is clear that σ_P exceeds the thermocharge σ_T by a factor a/λ which, for micron-size particles, is of the order of $a/\lambda \sim 100$.

The resulting electric field lines of a heated Janus colloid are shown in Fig 3.1 c: The far-field corresponds to the Seebeck field $\mathbf{E} = S\nabla T$, whereas the near-field depends strongly on the surface properties. At the conducting cap (the metal side), the parallel component vanishes within one Debye length. In order to relate the thermally induced charges and the thermoelectric field to the surface conductivity, we show in Fig. 3.5b and c how the Seebeck field of a constant temperature is deformed in the vicinity of a colloid with an insulating or conducting surface coating. Both differ significantly from the deformation of an applied electric field, which is shown in Fig. 3.5a. As a conclusion, we say that the behavior of the thermoelectric field at solid boundaries is very different from that of a voltage induced field.

3.6.3 Granular gold surface

The above discussion assumes a continuous gold cap, which does not always correspond to the actual experimental situation. For example, the cap of the particles used in Ref. [15] consists of a dense coverage of nano-sized gold grains, visible in scanning electron microscopy images [39] and illustrated in Fig. 3.6.

These grains do not connected to a continuous gold structures. Each grains forms an equipotential surface, and, as in the case of a continuous gold cap, the resulting parallel field vanishes within one screening length. As illustrated in Fig. 3.6, we see the existence of a potential jump between nearby grains; their cold and hot boundaries carry polarization charges which result in a strong electric field in the grain's spacing. As a consequence, the picture developed for micron-size conducting surfaces remains correct at the nanoscale. Because of the surface

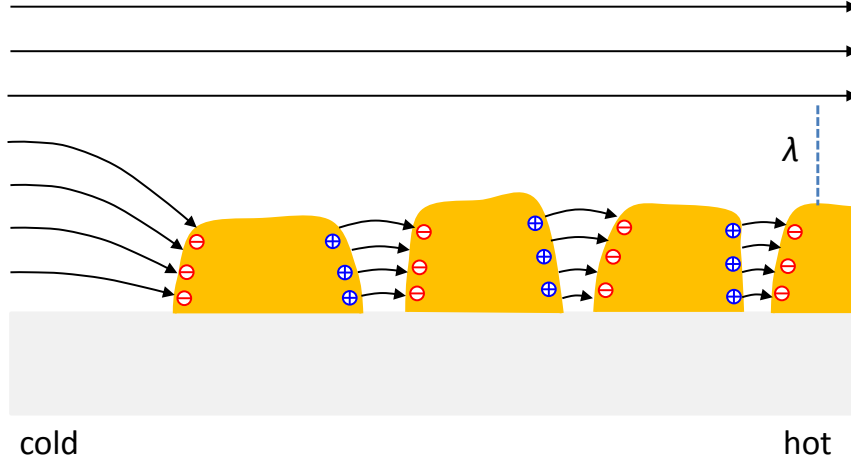


Figure 3.6: Parallel component E_{\parallel} of the thermoelectric field in the vicinity of a granular gold cap ($S > 0$). Each metal grain forms an equipotential surface and carries opposite polarization charges σ_P at its cold and hot sides. Like on the continuous cap in Fig. 3.1c, E_{\parallel} vanishes in a layer of about one screening length. On the insulating surface at the left, the field is given by (3.12).

roughness one may expect a somewhat smaller slip velocity than at a homogeneous cap.

3.6.4 Comparison with experiment

A recent experiment reported thermoelectric driving of hot silica particles with a granular gold cap [15]. Probing the particle's self-propulsion velocity in 10 mM solutions of NaCl, LiCl and NaOH, revealed a strong salt-specific effect, which agrees qualitatively with the Seebeck coefficients of these electrolytes, $S_{\text{NaCl}} > S_{\text{LiCl}} > S_{\text{NaOH}}$. When comparing to experimental findings, one has to add to v_s the thermo-osmotic and related contributions, subsumed in v_s^{osm} , which are of comparable magnitude but independent of the ion species [16].

Contrary to what was observed for passive polystyrene beads in an external temperature gradient [16], the experiments of Ref. [15] seem to indicate that the negative Seebeck effect of NaOH does not result in a change of sign of the self-propulsion velocity of an active particle. This could be related to the granular

gold surface, the properties of which could differ from the behavior derived for a continuous gold surface assumed in this paper. As another possible explanation, we mention the strong increase of v_s^{osm} with temperature, whereas the thermoelectric contribution was found to be rather constant [16].

3.7 Conclusion

The aim of this present study was to understand the nanoscale Seebeck effect for a hot metal nanostructure in contact with electrolyte solution. In other words, we studied the self-propulsion mechanism induced by the thermo-electrophoresis effect of an active particle. In this problem, the thermoelectric properties are studied by considering different surface geometry, i.e, the surface of the particle can behaves as an insulating or a conducting surface.

At the insulating surface, the diffuse layer consists of two contributions: The double-layer charge ρ_0 inducing by the surface charge σ_0 which is not affected by the Seebeck effect, and the non-uniform thermocharge ρ_T which is proportional to the surface excess temperature T_S . This temperature field increases, in the case of a Janus particle, from the passive hemisphere to the heated cap, resulting in a parallel component of the Seebeck field along the particle surface. On the conducting surface, the parallel temperature gradient induces polarization charge on the metal structure, which modify the double layer such that the parallel component of the electric field vanishes at the surface. Surprisingly, this does not affect the thermally induced slip velocity, which turns out to be identical on insulating and conducting surfaces.

In addition, our theoretical results agree qualitatively with a recent experiment [15]: When regarding specific-ion effects, the self-propulsion velocity shows a significant variation with the used salts NaOH, NaCl, LiCl. Taking into account these above points, we can conclude that the thermoelectric properties of hot Janus particles in an electrolyte solution depend strongly both on the material properties and the specific-ion effects.

Chapter 4

Hydrodynamic interactions in DNA thermophoresis

4.1 Introduction

The dynamics of polyelectrolytes is of considerable interest in a fields such as microfluidics and biotechnology applications [33]. Understanding their dynamics can be essential to perform properties of electrophoresis or thermophoresis of polyelectrolytes. In the past, the first models predicting the dynamics of polymer chain in solution was developed by Rouse and Zimm [34, 35]. In these theories, the polymer is modelled as a chain with a large number of spherical beads connected by springs. The main difference between these two models is the effect of hydrodynamic interactions which are absent in Rouse's model and present in Zimm's model. Consequently taking into account these hydrodynamic interactions between beads, the diffusion coefficient scale as: $D \propto N^{-\nu}$, where the Flory exponent $\nu = 0.6$ for real chains in good solvent [13]. This last equation shows that the diffusion coefficient of the polymer chain varies with the number of beads, i.e, it depends strongly on the molecular-weight.

In contrary, phoretic mechanism for polymers in a dilute solution is usually considered to be independent on the molecular-weight. This point was first discussed and confirmed by Giddings when studying thermophoresis of high polymers [12], and later by Brochard and de Gennes by showing that the hydrodynamic interactions have no effect on thermophoresis for polymers [25]. More recently, considerable progress has been made on DNA-phoresis; these results revealed, however, a

molecular-weight dependence on the mobility in the range where the persistence length $L \sim \lambda$ with λ the Debye screening length [36, 37]. Muthukumar confirmed this molecular-weight dependence and showed the importance of "hydrodynamic screening" on DNA phoresis [27, 28].

In this present chapter, we investigate in the hydrodynamic screening of DNA thermophoresis, and in particular we study the influence of hydrodynamic interactions in a dilute polyelectrolytes solution: In the polymer chain, a given molecular creates a flow field and drags its unit neighbor beads. This effect increases the velocity of the chain until it saturates at large distances well beyond the Debye screening length, where the drag forces exerted by charged monomers and the corresponding counterions cancel each other. We evaluated theoretically the thermophoretic mobility D_T of a polymer chain of n beads. This mobility shows, in function of the chain length, a non-monotonous behavior and consists of two contributions: a dielectrophoresis induced by permittivity gradient and the Seebeck effect. At the first time, we begin by studying about the hydrodynamic interactions arising during the mechanism process. At second, we give a detailed calculation of the phoretic coefficients and we discuss about the counterion condensation effect which strongly influences the thermophoretic mobility's behavior. At the end, we compare our theory with recent experimental result on single-stranded DNA [44].

4.2 Thermodynamic forces

Due to the presence of the temperature gradient, the system exerts lateral forces on the counterions surrounding the charged monomer which in turn moves the fluid with respect to the particle surface. The created force, called force density or thermodynamic force, results from the interactions at the solid-solvent interface, and his general expression reads as [51]

$$\mathbf{f} = -(\rho\psi + n_i k_B T) \frac{\nabla T}{T} - \frac{E^2}{2} \nabla \epsilon - n_i k_B T \frac{\nabla n_0}{n_0} + \rho \mathbf{E}_T, \quad (4.1)$$

where ϵ the solvent permittivity, n_0 the bulk salinity, $n_i = n_+ + n_-$ the excess ion density and $\rho = e(n_+ - n_-)$ the total charge density. The force density (4.1) describes the force exerted on the counterions cloud surrounding the charged monomer, and it's given in terms of quantities describing the electric double layer and the thermoelectric field. In Eq. (4.1), the terms proportional to $\propto \nabla T$ and

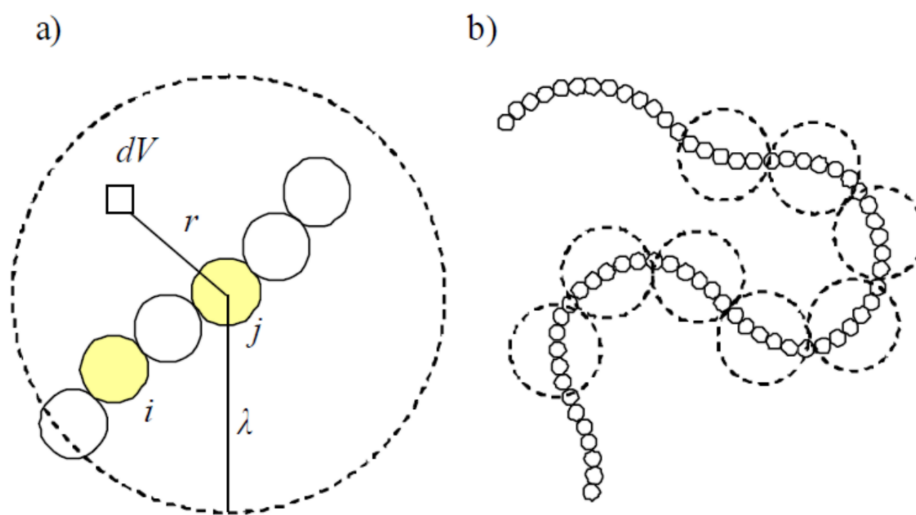


Figure 4.1: Schematic view of a charged polymer in an electrolyte solution. a) The drag on bead i consists of two contributions: First, the motion of bead j , driven by the force \mathbf{F} , creates a flow field $\mathbf{v}(\mathbf{r} - \mathbf{r}_j)$ and thus drags its neighbor i . Second, due to the force \mathbf{f} exerted by the bead j , the fluid element dV moves and in turn exerts a drag on bead i . These contributions cancel each other at distances well beyond the Debye length λ . b) At the scale of the Debye length, a polyelectrolyte is a rigid molecule; at short distances within λ , the spacing of two beads of radius a is well described by $r_{ij} = 2a|i - j|$.

$\propto \nabla n_0$ result from the osmotic pressure i.e the pressure of the excess density of mobile ions, the second term $\propto \nabla \varepsilon$ results from the divergence of the Maxwell stress tensor which describes the force exerted by the charged-monomer surface, and the last term $\rho \mathbf{E}_T$ describes the force exerted by the macroscopic thermoelectric field $\mathbf{E}_T = S \nabla T$ on the monomer's counterion density ρ [18].

All the terms in \mathbf{f} are of comparable magnitude but for small molecules, that is, for molecules's size a much more smaller than the screening Debye length λ , then the companions field \mathbf{E}_T and $\nabla \varepsilon$ dominate whereas the gradients ∇T and ∇n_0 are negligible. Thus the simplified expression of the density force becomes,

$$\mathbf{f} = -\frac{E^2}{2} \nabla \varepsilon + \rho \mathbf{E}_T, \quad (4.2)$$

where the first term is proportional to the thermally induced permittivity gradient $\nabla \varepsilon = (d\varepsilon/dT) \nabla T$, with the charged monomer's electric field E . Since the permittivity decreases with rising temperature, $d\varepsilon/dT < 0$, the surrounding water moves to the hot, as recently confirmed experimentally for thermoosmosis in a capillary [45]. By reaction, the molecule migrates toward the cold. The electrolyte Seebeck coefficient S is a salt-specific quantity that may take either sign, resulting in motion along the temperature gradient or opposite to it [16].

The density force given in Eq. (4.1) play also the rule of source term in the hydrodynamic Stokes equation. Now assuming that the electrostatic potential $e\psi$ is much more smaller than the thermal energy $k_B T$ ($e\psi \ll k_B T$) then the charge density ρ can be expanded in quadratic order in term of ψ as, $\rho \simeq -\varepsilon \psi / \lambda^2$. Inserting the number permittivity derivative $\tau = -d \ln \varepsilon / d \ln T$, the Debye screening length $\lambda^2 = 1/8\pi n_0 l_B$ the Debye length with $l_B = e^2/4\pi\epsilon k_B T$ the Bjerrum length, we can write the density force as a linear function of the thermal gradient,

$$\mathbf{f} = \left(\frac{\tau \epsilon E^2}{2k_B T} - \frac{\delta \alpha \epsilon \psi}{e \lambda^2} \right) k_B \nabla T. \quad (4.3)$$

The force density \mathbf{f} acts on the surrounding water and, by reaction, the molecular unit is subject to the opposite force $\mathbf{F} = -\int dV \mathbf{f}$ [51]. Thus the velocity field induced by the moving bead i at the position of its neighbor j , consists of two contributions,

$$\mathbf{v}(\mathbf{r}_{ij}) = \mathbf{G}(\mathbf{r}_{ij}) \cdot \mathbf{F} + \int \mathbf{G}(\mathbf{r}_{ij} - \mathbf{r}) \cdot \mathbf{f}(\mathbf{r}) dV, \quad (4.4)$$

where $\mathbf{G}(\mathbf{r}) = (1 + \widehat{\mathbf{r}}\widehat{\mathbf{r}})/8\pi\eta r$ is the Oseen tensor with the viscosity η and $\widehat{\mathbf{r}} = \mathbf{r}/r$ [52]. The first term describes the long-range velocity field $v \sim 1/r$ or “stokeslet” of a particle subject to an external force \mathbf{F} ; it gives rise to strong hydrodynamic effects on diffusion and sedimentation [13]. The second term is characteristic for phoretic motion; it may be viewed as the sum of stokeslet flows of strength $\mathbf{f}dV$ and centered at a distance \mathbf{r} from the particle. Since both E and ρ vanish well beyond the Debye length, the second term cancels the first one at large distances, $r_{ij} \gg \lambda$, whereas it is small for nearby beads.

4.3 Hydrodynamic interactions

We want here to study the influence of the hydrodynamic interactions in a dilute polyelectrolytes solution. Now consider a polyelectrolyte chain of n building blocks where each molecular bead of charge q results in a Debye-Hückel surface potential $\zeta = q/4\pi\epsilon a$, as illustrated in Fig. 4.1. Throughout this paper, we assume that the molecular size a is small compared to the Debye screening length λ . Unit i creates a flow field $\mathbf{v}(\mathbf{r} - \mathbf{r}_i)$ in the surrounding fluid and thus drags its neighbor j . Then the overall velocity \mathbf{u} of the chain is given by the sum of the monomer contribution \mathbf{u}_1 and the mutual advection,

$$\mathbf{u} = \mathbf{u}_1 + \frac{1}{n} \sum_{i,j \neq i} \langle \mathbf{v}(\mathbf{r}_{ij}) \rangle, \quad (4.5)$$

where the angular brackets $\langle \cdot \cdot \rangle$ indicates the configurational average with respect to $\mathbf{r}_{ij} = \mathbf{r}_j - \mathbf{r}_i$. Before computing Eq. (4.5) and finding the velocity of the chain, one have to specify the flow field $\mathbf{v}(\mathbf{r}_{ij})$ and all the physical forces arising during the mechanism process. In order to simplify the second term in the velocity \mathbf{u} , the configurational average is done with the equilibrium distribution function. The later being isotropic, the only finite component of the mean drag velocity is along the temperature gradient, and the tensor equation in (4.4) is simplified to a scalar one where the Oseen tensor is replaced by its diagonal part by $G(r) = 1/6\pi\eta r$. Inserting the expression of the density force and averaging over the position i of the polymer chain, the Eq. (4.5) becomes

$$u = u_1 + \frac{1}{n} \sum_{i,j \neq i} \int \langle G(|\mathbf{r}_{ij} - \mathbf{r}|) - G(r_{ij}) \rangle f(\mathbf{r}) dV, \quad (4.6)$$

The second term in parenthesis depends on the details of the counterion distribution; for later use we expand the pre-average Oseen tensor in term of Legendre Polynomials $P_k(\cos \theta)$, with $\cos \theta = \widehat{\mathbf{r}}_{ij} \cdot \widehat{\mathbf{r}}$,

$$G(|\mathbf{r}_{ij} - \mathbf{r}|) = \frac{1}{6\pi\eta} \sum_{k=0}^{\infty} P_k(\cos \theta) \frac{h_{ij}^k}{H_{ij}^{k+1}}, \quad (4.7)$$

where $h_{ij} = \min(r, r_{ij})$ denotes the smaller of the distances r and r_{ij} , and $H_{ij} = \max(r, r_{ij})$ the larger one.

Now the problem remain to compute the volume integral in Eq. (4.6), and, in other word, to evaluate Eq. (4.7) with an appropriate counterion distribution. We start by evaluating the monomer's electrical potential ψ with the corresponding electric potential $E = -\nabla\psi$ which are both screened. In this case, the electrostatic potential of a single bead of valence \widehat{z} is well described by the Debye Hückel approximation,

$$\psi = \zeta \frac{a}{r} e^{-r/\lambda}, \quad (4.8)$$

where the single bead surface potential $\zeta = -\widehat{z}e/4\pi\epsilon a$, which we assume to be negative.

By applying $E = -d\psi/dr$ we obtain easily the radial monomer's electric field. Inserting Eq. (4.8) into Eq. (4.6), one finds the only finite contribution stems from the term $k = 0$ in Eq. (4.6), and the remainder vanishes for an isotropic screening cloud. Assuming that the particle's radius a is much smaller than the Debye length λ , and the quantity na be of the order of λ , the volume integral in Eq. (4.6) is readily performed by doing a first order development in term of a/λ . We obtain,

$$\int \langle G(|\mathbf{r}_{ij} - \mathbf{r}|) - G(r_{ij}) \rangle f(\mathbf{r}) dV = \tau \frac{\epsilon a^2 \zeta^2}{6\eta T} \left\langle \frac{e^{-2r_{ij}/\lambda}}{r_{ij}^2} \right\rangle - 2S \frac{\epsilon a \zeta}{3\eta} \left\langle \frac{e^{-r_{ij}/\lambda}}{r_{ij}} \right\rangle, \quad (4.9)$$

where $S = \delta\alpha k_B/e$ is the electrolyte Seebeck coefficient. This last equation characterizes the hydrodynamic interactions between monomers and shows the latter is exponentially screened.

To find the complete expression of the chain's velocity, we begin by simplifying the configurational average by treating the molecules as rigid rods such that the distance of beads i, j simplifies to $r_{ij} = |i - j|d$, where d the distance between two

consecutive beads. As a consequence, the double sum is replaced by the double integral over i and j . So we have to compute,

$$u = u_1 + \frac{1}{n} \left\{ \tau \frac{\epsilon a^2 \zeta^2}{6\eta T} \iint_1^n didj \left(\frac{e^{-2|i-j|d/\lambda}}{|i-j|^2 d^2} \right) - 2S \frac{\epsilon a \zeta}{3\eta} \iint_1^n didj \left(\frac{e^{-|i-j|d/\lambda}}{|i-j|d} \right) \right\} \nabla T. \quad (4.10)$$

Eliminating the absolute value and computing the double integral over i and j , one finds finally

$$\mathbf{u} = \frac{\zeta^2}{3\eta} (1 + \chi_\epsilon) \nabla \epsilon + \frac{2\epsilon \zeta}{3\eta} (1 + \chi_S) \mathbf{E}_T. \quad (4.11)$$

where the quantities χ_ϵ and χ_S account for hydrodynamic interactions (see Fig. 4.2) With $\chi_\epsilon = 0 = \chi_S$ one has the explicit expression for the monomer velocity \mathbf{u}_1 .

The hydrodynamic correction factor for the motion driven by the permittivity gradient reads,

$$\chi_\epsilon = \frac{a^2}{d^2} \left((1 + 2n\hat{d}) \frac{E_{2\hat{d}} - E_{2n\hat{d}}}{n} + e^{-2\hat{d}} - \frac{e^{-2n\hat{d}}}{n} \right), \quad (4.12)$$

with the shorthand notation $E_x = \text{Ei}(-x)$ for the exponential integral function which is defined as

$$\text{Ei}(x) = \int_{-\infty}^x \frac{e^{-u}}{u} du,$$

and $\hat{d} = d/\lambda$ for the ratio of the monomer length and the Debye length. For the Seebeck term we find

$$\chi_S = \frac{2a}{d} \left(E_{n\hat{d}} - E_{\hat{d}} + \frac{e^{-n\hat{d}} - e^{-\hat{d}}}{n\hat{d}} \right), \quad (4.13)$$

The factor 2 in the exponential and Ei functions in χ_ϵ arises from the screening factor of the force density, $E^2 \propto e^{-2r/\lambda}$, whereas the factors in χ_S are related to the decay of the screening cloud, $\rho \propto e^{-r/\lambda}$. The Seebeck term χ_S can be seen as an electrophoretic mobility which is identical to Muthukumar result [27], albeit with the bead distance d instead of Kuhn length l . In the expression of the chain

velocity \mathbf{u} , we detect two terms: a dielectrophoresis induced by the permittivity gradient $\nabla\epsilon$ and the electrolyte Seebeck effect induced by the thermoelectric field $\mathbf{E}_T = S\nabla T$. The influence of these two terms are shown in Fig. 4.2 where we plotted the quantities χ_ϵ and χ_S as a function of the molecular weight. Both vanish for monomers, $n = 1$, whereas for long molecules they tend toward the constants $\chi_\epsilon^\infty = (a/d)^2(2\hat{d}E_{2\hat{d}} + e^{-2\hat{d}})$ and $\chi_S^\infty = -2(a/d)E_{\hat{d}}$.

4.4 Counterion condensation

In addition to hydrodynamic interactions arising during the dynamics of polyelectrolytes, we observe another phenomenon which is called counterion condensation: due to Coulomb interactions, a strong charged polyelectrolyte exerts a powerful attraction on counterions which partly condense on the polymer until its line charge density is reduced to the critical value e/l_B [53]. The condensed ions move with the polymer chain, and the uncondensed mobile ions present in the ionic atmosphere are well treated by the Debye-Hückel theory. Because of this condensation effect, everything changes even the effective charge per monomer $q = -\hat{z}e$. This charge remains unknown, and to overcome this difficulty, we estimate its value by taking into account its reduction along the bare charge n . Thus we consider for simplicity

$$\hat{z} = \xi^{-1} + \frac{1 - \xi^{-1}}{1 + \beta_n}, \quad (4.14)$$

where $\xi = l_B/d$ is called the Manning parameter, and $\beta_n = (n^2 - 1)n_0^{-2}$ with n_0 an arbitrary constant value. This constant value enhances the precision of the analytical curve, and $n_0 = 80$ we obtain best fits for the experimental data (see Fig. 4.2). The parameter ξ models the counterion condensation effect, in the sense that, if $\xi > 1$ the condensation effect takes place because the Coulomb interaction is very strong and dominates the thermal one; but if $\xi < 1$, meaning that the bead spacing d is larger than the Bjerrum length $l_B \simeq 7\text{\AA}$, then the electrostatic forces acting on the chain are very weak compared to the thermal forces, and thus the condensation effect does not occur in this case.

However, the condensation effect is relevant for polyelectrolytes because the molecules are strongly charged and the bead spacing distance d is something between 3 and 4 \AA . The valency \hat{z} of the effective charge given in Eq. (4.14) satisfies completely the Manning's prediction, in the sense that, for a monomer the quantity

β_n vanishes, one has $\hat{z} = 1$, and for long chains β_n goes to infinity, thus the resulting effective charge valence decrease along the barre charge until it converge to $\hat{z} = \xi^{-1}$.

4.5 Results and comparison with experiment

The thermophoretic mobility is defined from the drift velocity relation $\mathbf{u} = -D_T \nabla T$. From this equation, the thermophoretic mobility reads,

$$D_T = \tau \frac{\epsilon \zeta^2}{3\eta T} (1 + \chi_\epsilon) - S \frac{2\epsilon \zeta}{3\eta} (1 + \chi_S). \quad (4.15)$$

We can obtain a detailed expression by inserting the valence of the effective charge \hat{z} and the Bjerrum length l_B ,

$$D_T = \frac{k_B}{12\pi\eta a} \left\{ \hat{z}^2 \frac{l_B}{a} (1 + \chi_\epsilon) + 2\hat{z} (1 + \chi_S) \hat{S} \right\}, \quad (4.16)$$

where the parameter $\tau = -d \ln \epsilon / d \ln T \approx 1.4$ which arises from the permittivity gradient, and the dimensionless Seebeck coefficient $\hat{S} = S(e/k_B)$. This thermophoretic mobility is valid for small monomers, that is, for monomer's size much more smaller than Debye length. For monomers the mobility is independent of the Debye length, whereas for longer chains, the correction factors give rise to complex dependencies on λ and n . This mobility shows also two contributions which are plotted as a function of n and shown in Fig. 4.2. These contributions have a non-monotonuous behavior, both they reach a maximum and decrease until they reach a finite constant value for large n ; for typical parameters of DNA in weak electrolyte, the permittivity term shows an overall decrease, $\hat{z}^2(1 + \chi_\epsilon^\infty) < 1$, whereas the Seebeck term is enhanced, $\hat{z}(1 + \chi_S^\infty) > 1$. As a consequence, the thermophoretic mobility has the same behavior. The explanation of this variation is nothing else that the first increase result from the hydrodynamic interactions between monomers then the decrease is caused by the reduction of the effective charge inducing by the condensation effect.

Our theory gives the thermophoretic mobility D_T in Eq. (4.16), whereas experiment often probe the Soret coefficient $S_T = D_T/D$, where the diffusion coefficient $D = k_B T / 6\pi\eta R_h$ is determined by the hydrodynamic radius R_h of the molecules.

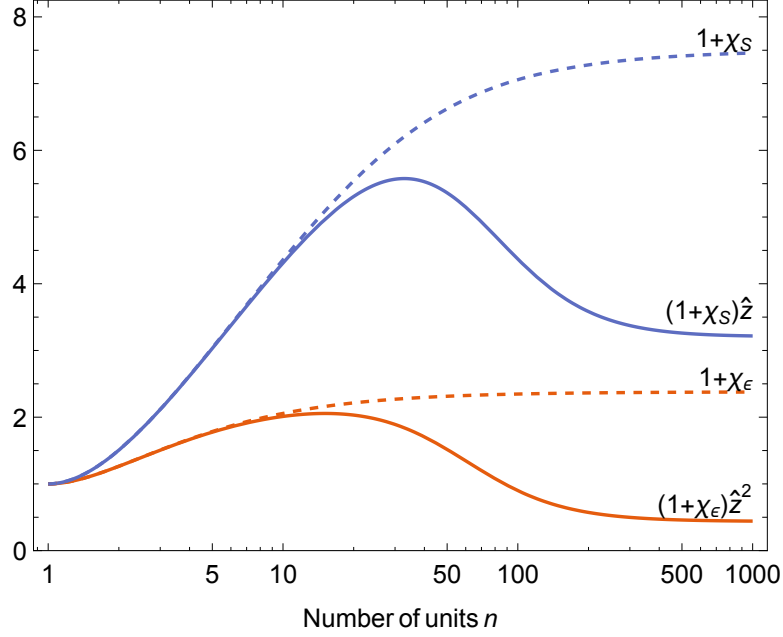


Figure 4.2: Variation of the two contributions to the thermophoretic mobility D_T , the dielectrophoretic coefficient $\sim 1 + \chi_\epsilon$ and the Seebeck effect $\sim 1 + \chi_S$, depending on the molecular weight. The parameters used for this plot: monomer's size $a = 4.25\text{\AA}$, monomer's distance $d = 3\text{\AA}$ and Debye length $\lambda = 5\text{ nm}$. The factors, χ_ϵ and χ_S characterize the hydrodynamic interactions and increase with the chain length n (dashed line), \hat{z}^2 and \hat{z} result from the counterion condensation which reduce the mobility (Solid line).

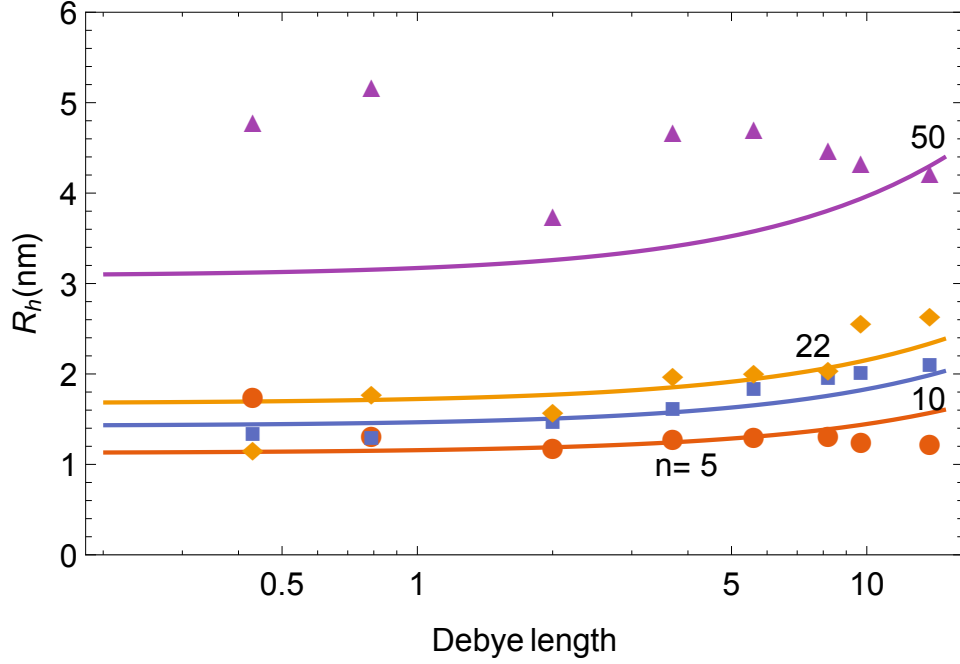


Figure 4.3: The variation of the hydrodynamic radius $R_h = R(n) [1 + (\lambda - 7) / 42]$ where we took from the paper [55] and $R[n](\text{nm})$ is an adjustable parameter with n is the number of beads in the polymer chain. We took for this parameter: $R(5) = 1.35$, $R(10) = 1.71$, $R(22) = 2.01$, $R(50) = 3.7$, $R(80) = 4.74$.

Unfortunately, for short molecules, there is no simple and generally formula for the hydrodynamic radius. To overcome this difficulty, we have estimated the value hydrodynamic radius in the simple way by,

$$R_h = R(n) \left[1 + \frac{\lambda - \lambda_0}{L} \right], \quad (4.17)$$

where λ_0 , L are an arbitrary constant lengths, and $R(n)$ be an adjustable parameter which describes also the measured mean value of the hydrodynamic radius. The hydrodynamic radius is modeled in Eq. (4.17) in order to determine the diffusion coefficient D and the Soret coefficient S_T , and to agree with recent experimental measurement [55]. Fig. 4.3 shows the measured values of the hydrodynamic radius R_h in function of the Debye length, which agree slightly with the analytical one from Eq. (4.17). The values for $n = 10$ and 22 slightly increase with the Debye

Debye length λ (nm)	Soret coefficient S_T ($10^{-2}/\text{K}$) at $T = 15^\circ\text{C}$					
	2 mer	5 mer	10 mer	22 mer	50 mer	80 mer
2.16	0.78	1.19	1.86		2.11	3
3	1.03	1.49	2.12	2.86	3.10	3.27
4.16	1.15	1.9	2.7		3.69	4.6
5.2	1.29	1.89	2.89	3.8	5.19	4.8
6.16	1.45	1.89	2.59	4.2	5.79	6.21
7	1.5	1.89	3.2	4.41	5.8	6.31
8	1.43	2.25	3.07	4.44	6.58	6.29
9.74	1.48	2.09	3.4	4	7.1	6.09
11.25	1.45	2.2	3.29		8.81	5.21

Table 4.1: Experimental value of ssDNA Soret coefficient in function of the Debye length at the corresponding chain length: 5 monomers, 10 monomers, 22 monomers, and 80 monomers.

length, as expected from the increased stiffness in weak electrolyte. The data for $n = 5$ and 50 show a slight decrease and significant scatter.

In Fig 4.4 we compare our theory with the experimental Soret data for single-stranded DNA as a function of the Debye length λ , taken from Ref. [44] and given in Table 4.1. The theoretical curves are calculated with Eq. (4.16) and a simple model for the diffusion coefficient D , as described above. The best agreement with the data is obtained when retaining in Eq. (4.16) the permittivity-gradient term only, that is, for zero Seebeck coefficient, $\widehat{S} = 0$. The increases of S_T with the Debye length arises mainly from the hydrodynamic correction χ_ϵ . For short chains, that is for $n < 30$, the variation with n is of purely hydrodynamic origin, whereas for larger chains counterion condensation plays an important role, as is clear from Fig. 4.2.

In order to clearly display the effect of hydrodynamic interactions, we plot in Fig. 4.5 the thermophoretic mobility in (4.16) as a function of the molecular-weight n . The experimental points are obtained from $D_T = DS_T$, with the measured coefficients S_T and D which are determined from the estimated function for the hydrodynamic radius R_h given in Eq. (4.17). The theoretical curves are calculated with the permittivity only ($\widehat{S} = 0$). The initial increase of the data up to $n = 22$ agree quantitatively with the relation (4.12), thus providing strong evidence for the role of hydrodynamic interactions. The maximum and the subsequent decrease

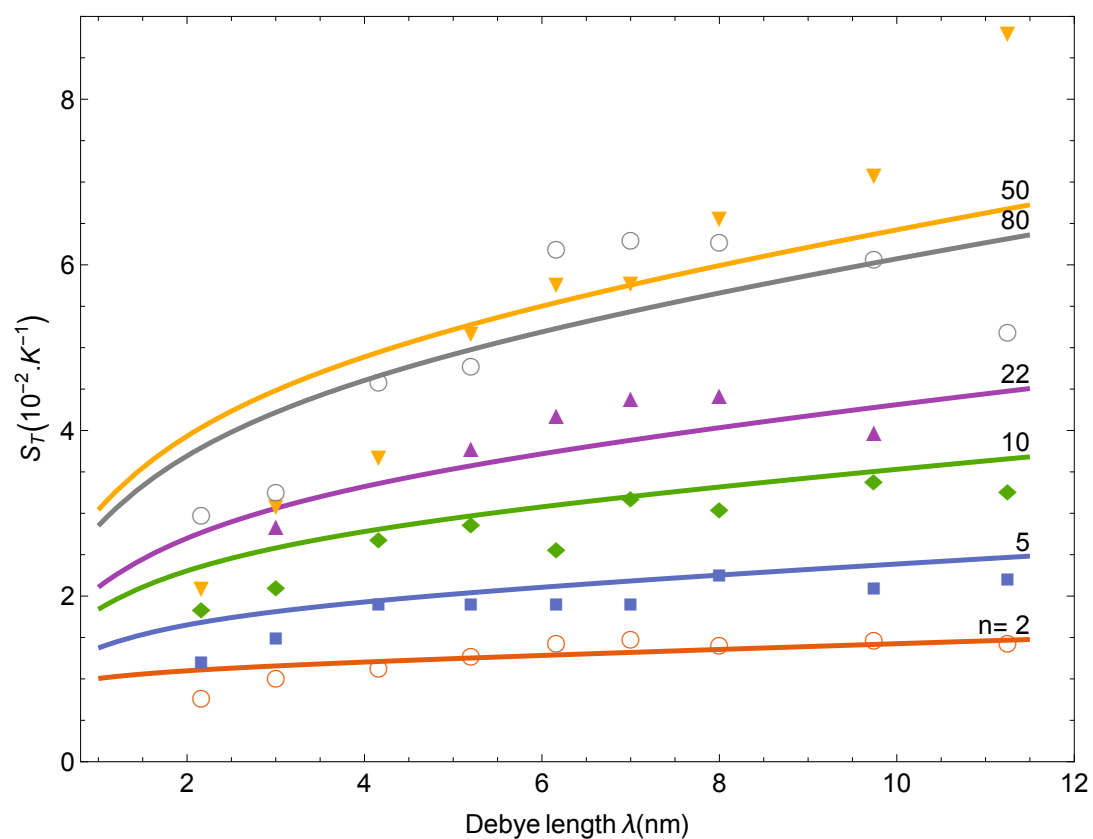


Figure 4.4: Variation of experimental and analytical Soret coefficient S_T in function of the Debye length λ . The parameters used here for the two graphs are: the monomer's size $a = 4.25 \text{ \AA}$ and distance between monomer $d = 3 \text{ \AA}$, the reduced Seebeck coefficient $\hat{S} = 0$.

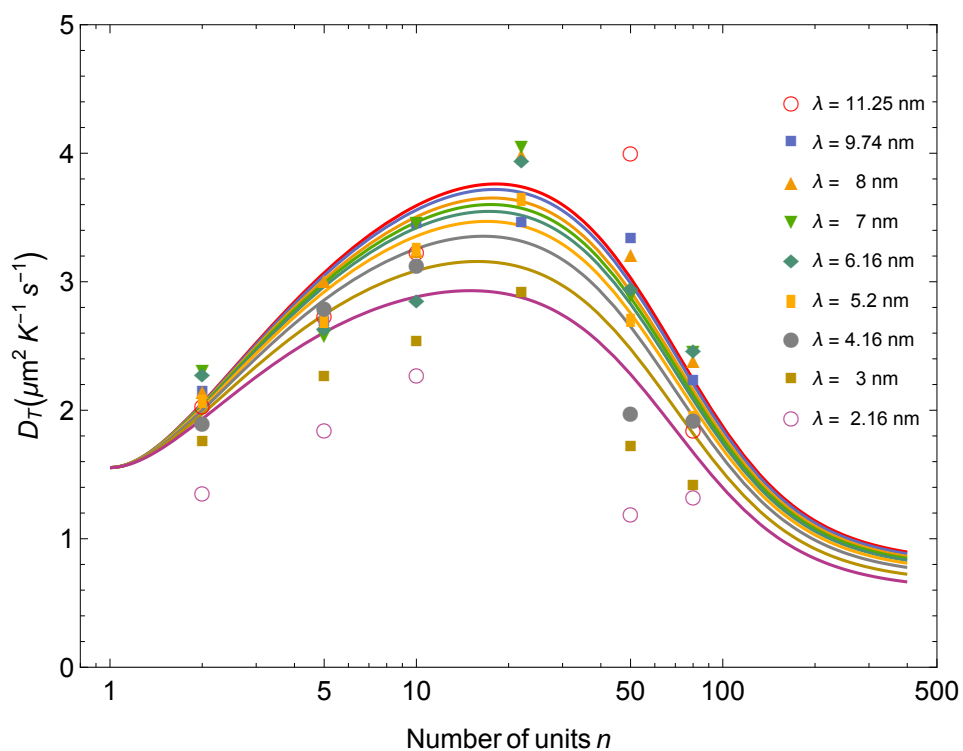


Figure 4.5: Variation of experimental and analytical: a) thermophoretic mobility D_T in function of the chain length n . The parameters used here for the two graphs are: the monomer's size $a = 4.25 \text{ \AA}$ and distance between monomer $d = 3 \text{ \AA}$, the reduced Seebeck coefficient $\hat{S} = 0$.

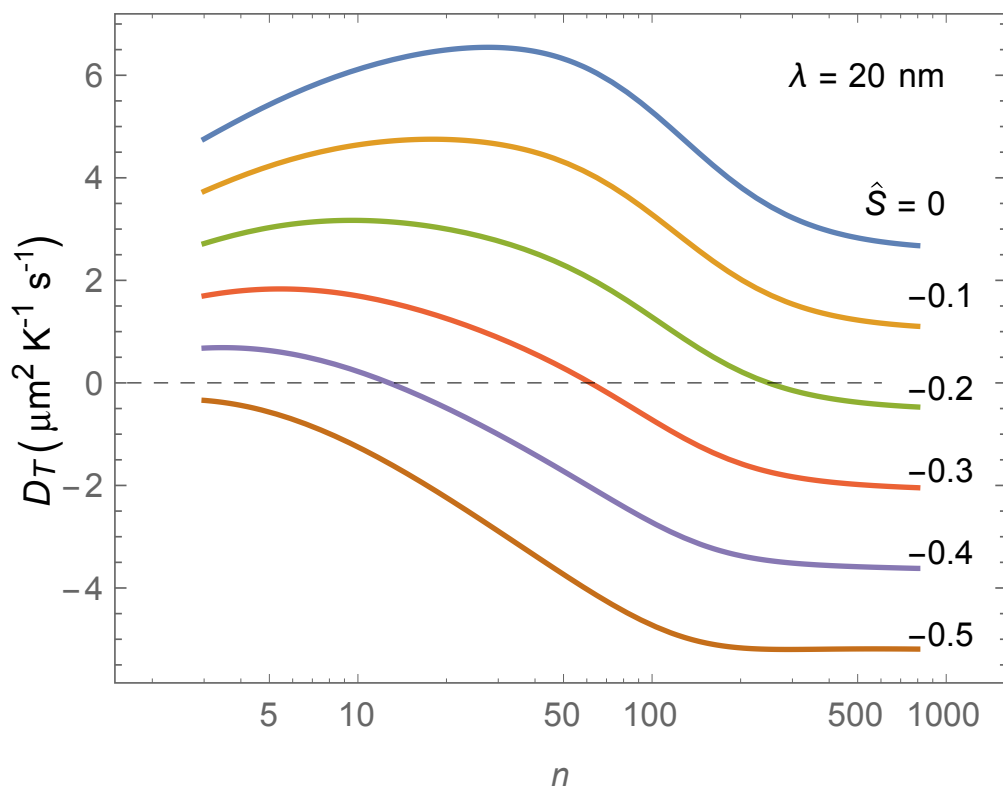


Figure 4.6: Thermophoretic mobility D_T as a function of the chain length n , for different values of the dimensionless Seebeck coefficient \hat{S} . For negative \hat{S} the thermoelectric field in (4.11) drives the molecules toward the hot, whereas the permittivity gradient points toward the cold. Since the latter dominates for short molecules and the latter for long ones, D_T changes sign as the n increases.

are well described by counterion condensation according to (4.14). Adding a significant thermoelectric contribution, i.e, increasing the reduced Seebeck coefficient \widehat{S} , would not improve the quality of the fit, quite on the contrary. This indicates that the Seebeck field in NaCl solution is small, confirming a previous analysis of thermophoretic measurements on polystyrene beads [16].

The electrolyte Seebeck effect was discarded in the above analysis of Soret data in NaCl solution. In Fig 4.6 we plot the complete thermophoretic mobility D_T as a function of the molecular-weight n , for several values of the dimensionless Seebeck coefficient \widehat{S} . As the most striking feature, for negative \widehat{S} the superposition of the two contributions in (4.16) may result in a change of sign of D_T . From Fig. 4.2 it is clear that for short chains, the permittivity gradient term prevails, whereas for longer molecules the Seebeck term dominates because of its much larger hydrodynamic factor χ_S . The resulting velocity difference could be used for specific accumulation of one component at a heated spot. For example, in an electrolyte with $\widehat{S} = -0.3$, the permittivity gradient dominates for short molecules ($n < 50$) which move to the cold accordingly, whereas longer chains are driven to the hot by the thermoelectric field.

4.6 Conclusion

The objective of this chapter was to discuss about the effects of hydrodynamic interactions and thermoelectric field occurring during the thermophoresis mechanism for DNA in electrolyte solution. As a summary of our main result, we start with the non-monotonous behavior of the thermophoretic mobility D_T which consists of two contributions: The motion induced by the permittivity gradient, that is the dielectrophoretic term χ_ϵ ; and the one induced by the Seebeck field χ_S . These two contributions have the same behavior: With increasing the chain length n , it presents a first increase resulting from the hydrodynamic interactions, and a decrease caused by the counterion condensation. For longer chains, that is for large n , the mobility D_T presents a limit which is obtained by letting $\chi \rightarrow \chi^\infty$ and $\widehat{z} \rightarrow \xi^{-1}$. This limit does not depend on the molecular-weight n , and does not vanish for high salinity or small Debye length, contrary to what was observed for micron-size colloidal particle [16].

In addition, the comparison of our theoretical results with the experimental data, shown in Fig. 4.4 and 4.5, reveals a strong dependence on the molecular-weight, which arises from the interplay of the hydrodynamic interactions and the

condensation effect. Finally, the change of sign of the mobility D_T depend on the negative value of the Seebeck coefficient S ; and in a physical term, it results from the interplay between the dominant driving forces: The thermally induced permittivity gradient and the Seebeck field with a negative Seebeck coefficient.

Chapter 5

Ion dynamics: time dependent effect

In section 3, we studied the thermoelectric properties of a metal capped colloid particle moving in a electrolyte solution. In that studies, all the physical properties are derived in the stationary state where the system is independent of time. Thus in this chapter, we will study the ion dynamics properties, and in other words the electrolyte Seebeck effect in the non-stationary state. We will also try to find the ion diffusion time scale and discuss about its effect on thermophoresis .

5.1 Charge conservation equation

In electrolyte solution, when ion-species are influenced by a non-uniform temperature gradient, thus results in an ion current J_{\pm} which is detailed in section 2. We define the total ion current by $\mathbf{I} = e(\mathbf{J}_+ - \mathbf{J}_-)$ and by linearizing, his expression becomes,

$$\mathbf{I} = -\varepsilon D \left\{ \nabla^2 \mathbf{E} - \frac{1}{\lambda^2} (\mathbf{E} - S \nabla T) \right\}, \quad (5.1)$$

where ε the solvent permittivity and $D = (D_+ + D_-) / 2$ the ion diffusion coefficient (more details in Appendix D). We want here to write the equation satisfied by the thermoelectric field in the non steady state. We start by the charge conservation equation related the total ion current \mathbf{I} and the charge density $\rho = e(n_+ - n_-)$,

$$\partial_t \rho + \text{div } \mathbf{I} = 0. \quad (5.2)$$

Applying Gauss's law $\text{div } \mathbf{E} = \rho/\varepsilon$, one obtains the equation describing the evolution of the generated electric field inside and outside the particle's electric double-layer,

$$\partial_t \mathbf{E} = D \left(\nabla^2 \mathbf{E} - \frac{1}{\lambda^2} (\mathbf{E} - S \nabla T) \right). \quad (5.3)$$

This last equation results from the charge conservation equation and characterizes the behavior of the electric field in the non-stationary state. When we put $\partial_t E = 0$, we find the equation (3.6) given in section 2 and section 3 where the system reaches the stationary state. The equation given in (5.3) is called reaction-diffusion equation where the right hand side describes the creation of the electric field, the left hand side characterizes the term of diffusion and the term $S \nabla T$ plays the rule of source for the thermoelectric field. To study the dynamics of colloid particle in an electrolyte solution, we will try to solve the reaction-diffusion equation in (5.3) and find the generated electric field in all state.

5.2 Effect on Janus particle

Consider a half-metal covered Janus colloid of radius a and centered at $\mathbf{r} = 0$. The self-generated temperature gradient is asymmetric due to half-metal absorption and remains always in the stationary state due to faster heat diffusion. Here we consider a particle with no surface charge, i.e, we are in the case of an insulating uncharged surface. To have simple computations, we define the reduced electrostatic potential by the relation $\mathbf{E} = -S \delta T \nabla \psi$, then the advection-diffusion equation becomes

$$\frac{\partial \psi}{\partial t} = D \left(\nabla^2 \psi - \frac{1}{\lambda^2} (\psi - T_l) \right), \quad \mathbf{r} > \mathbf{r}_0, \quad (5.4)$$

$$\mathbf{n} \cdot \nabla \psi = 0, \quad \mathbf{r} = \mathbf{r}_0, \quad (5.5)$$

where $r_0 = a$ the particle radius, and $T_l(\mathbf{r}) = (T(\mathbf{r}) - T_0)/\delta T$ is the reduced temperature field with $T(\mathbf{r})$ the self-generated temperature field [56]. For $r > a$, the reduced temperature field reads

$$T_l = \sum_{n=0}^{\infty} t_n P_n(c) \left(\frac{a}{r} \right)^{n+1} \quad (5.6)$$

where $c = \cos \theta$ and P_n the Legendre polynomial, and the coefficients t_n are given by, $t_{2k} = -t_{2k+1} = (-1)^k / \pi (2k + 1)$, except the first coefficient $t_0 = 1/2 + 1/\pi$.

The boundary condition in (5.5) says that the normal component of the electric field vanishes at the particle surface. The partial differential equation is solving by the Laplace transform with no initial condition, and by expanding the solution in first order in term of λ/a , with $\lambda \ll a$, one finds, outside of the particle for $r > a$, the electrostatic potential as

$$\psi(\mathbf{r}, t) = \psi(\infty) (1 - e^{-t/\tau_{\text{ion}}}), \quad (5.7)$$

where $\psi(\infty)$ is the potential in the steady state where the time exponential factor vanishes. Applying the relation $\mathbf{E} = -S\delta T \nabla \psi$, one can find easily the corresponding electric field (for more details see Appendix E). In Eq. (5.7) the quantity

$$\tau_{\text{ion}} = \frac{\lambda^2}{D}, \quad (5.8)$$

represents the characteristic time scale expressing the time of ion diffusion over the screening length. This time scale characterizes also the particle relaxation time, i.e, the time which the particle start moving. For typical values of the diffusion coefficient $D \sim 10^{-9} \text{ m}^2/\text{s}$ and the Debye length $\lambda = 50 \text{ nm}$, the relaxation time is in the order of $\tau_{\text{ion}} \sim \mu\text{s}$. Important to note that this ion diffusion time scale is by several order of magnitude greater than the thermal and hydrodynamic time scales which are, respectively, given by $\tau_{\text{th}} = \lambda^2/\alpha$ and $\tau_{\text{hy}} = \lambda^2/\nu$ with the heat diffusivity $\alpha \sim 10^{-7} \text{ m}^2/\text{s}$ and $\nu \sim 10^{-6} \text{ m}^2/\text{s}$ the kinetics viscosity. This last point tell us at which moment the particle start moving and enable us to discuss in more detail the effect of this relaxation time on thermophoresis.

5.3 Effect on thermophoresis

In the previous section, we discussed about the Seebeck effect in the non-steady state and computed the ion diffusion time scale τ_{ion} . In this present section we will study by details the time-dependent effect on the thermophoretic motion of particles. The particle's slip velocity can be written as,

$$v_s(t) = v_s^{\text{el}}(1 - e^{-t/\tau_{\text{ion}}}) + v_s^{\text{osm}}(1 - e^{-t/\tau_{\text{th}}}), \quad (5.9)$$

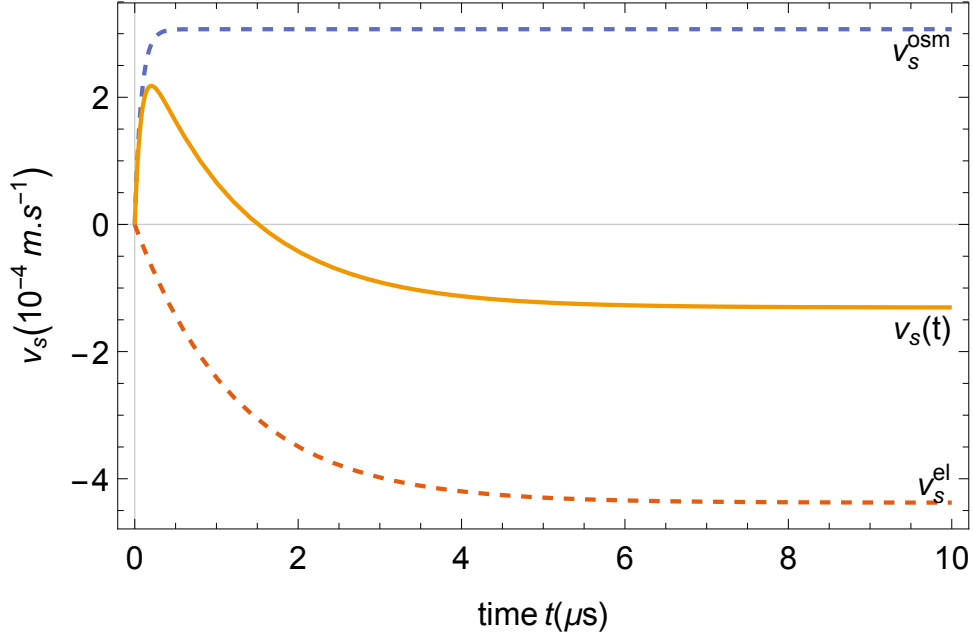


Figure 5.1: Time-dependent slip velocity v_s as the sum of the thermoelectric slip velocity v_s^{el} and the thermo-osmotic slip velocity v_s^{osm} . The plots are done in the interval of time $t = 0$ to $t = 10\mu\text{s}$ and with the fixed parameters: $S = -200\mu\text{V}/\text{K}$ for NaOH solution, $a = 1\mu\text{m}$, $\lambda = 50\text{nm}$, the surface potential $\zeta = -70\text{mV}$.

and which consists of two contributions: the time-dependent thermo-osmotic slip velocity v_s^{osm} and the thermoelectric slip velocity v_s^{el} . The thermo-osmotic slip velocity v_s^{osm} sets in on the heat-diffusion time scale $\tau_{\text{th}} \sim 10$ nanoseconds. The Seebeck effect requires ion diffusion which occurs on the time scale τ_{ion} that may attain a microsecond. Since in many instances, the thermoelectric slip velocity v_s^{el} is stronger and carries the opposite sign [17, 16], the onset of the Seebeck effect could even result in a reversal of the direction of motion.

5.4 Conclusion

The aim of this small chapter was to discuss about the dynamics of ions occurring once a temperature gradient is present in the system. In other words, we studied the time dependent effect, i.e, when the system is not in the stationary state. For that

we started by the charge conservation equation which rely the charge density ρ and the current caused by the diffusion of ion. The solution of this reaction-diffusion equation gives rise to the non-stationary thermoelectric field \mathbf{E} and the characteristic time scale for ion diffusion τ_{ion} . This time scale characterizes also the particle relaxation time. Indeed, this ion-diffusion time scale is by several order of magnitude greater than the thermal and hydrodynamic time scale. As a consequence, we observed a change of behavior in the motion of particle during the first milliseconds. This variation can be seen in the expression of the slip-velocity which consists of two different contributions: The time-dependent thermoelectric and thermo-osmotic slip-velocity, $v_s^{\text{el}}(t)$ and $v_s^{\text{osm}}(t)$, which set in on the ion-diffusion time scale $\tau_{\text{ion}} \sim 1\mu\text{s}$ and the heat-diffusion time scale $\tau_{\text{th}} \sim 10\text{nanoseconds}$, respectively. In Fig. 5.1, we showed the evolution of these two contributions in function of time, and, as the result, we found that the time-dependent thermoelectric slip-velocity dominates over the thermo-osmotic one. This last point shows how the Seebeck effect takes considerably an important place on the direction of motion of colloids in electrolytes.

Chapter 6

Summary and conclusion

This thesis was elaborated in order to study the nanoscale Seebeck effect at hot metal nanostructure. The electrolyte Seebeck effect is an important and powerful phenomenon on the transport mechanism for colloids or polyelectrolytes. To achieve completely this work, we organized this thesis in different chapters: The first two chapters was an introducing part of our work, where in chapter 1 we presented in detail different class of phoretic transport mechanism such as electrophoresis, diffusiophoresis and thermophoresis. Among these transports mechanisms, the motion induced by thermophoresis for hot colloids in electrolyte solution and for polyelectrolytes was studied in this present thesis. In electrolytes systems, the thermophoresis mechanism is not only caused by the thermally-induced salt gradient but also by the electrolyte Seebeck effect. The origin of this electrolyte Seebeck was presented and detailed in chapter 2.

After introducing the electrolyte Seebeck effect in 1-Dimension and 3-Dimension in chapter 2, we go to more complexes geometries in chapter 3 and we tried to understand how the electrolyte Seebeck effect behaves when the particle's surface varies from an insulating to a conducting surface. In this chapter, we tried also to understand how the change of behavior of the electric properties at an insulating and conducting surfaces can affect the induced slip-velocity v_s , and at the end we computed the resulting particle drift velocity \mathbf{u} . As a main result of this part, we found that: Near the insulating surface, the parallel component of the electric field E_{\parallel} is finite, whereas at an conducting surface carrying an high electrical conductivity, the isopotential condition imposes a polarization charge which modifies the double-layer potential such that its gradient cancels the thermoelectric field

at this surface, thus the parallel electric field vanishes. Surprisingly, the change of behavior of the thermoelectric field in function of the electrical conductivity does not affect the thermally-induced slip-velocity. This slip-velocity is identical at the insulating and conducting surfaces. As a consequence, the particle's drift velocity, resulting from the configurational average of the slip-velocity, also does not depend on the material properties but his sign vary strongly with the salt composition used NaOH, NaCl or LiCl. These above theoretical results have intensively revealed how both material properties and specific-ion effects can modify thermoelectric properties near a surface of a hot Janus colloid in an electrolyte solution.

Another important result for this work was presented in chapter 4, where we studied hydrodynamic interactions in thermophoresis for polyelectrolytes. In this chapter, we evaluated theoretically the thermophoretic mobility D_T , which arises from mutual advection of the n repeat units of the molecular chain. This mobility was studied in term of series expansion for the Oseen tensor. The two main physical phenomena occurring during DNA thermophoresis mechanism are the hydrodynamic interactions between monomers and the counterion condensation. Taking into account these phenomena, we found, as the main result, the thermophoresis D_T has a non-monotonous behavior and consists of two contributions: The first one is the motion induced by the permittivity gradient, that is the dielectrophoretic term χ_ε ; and the second one is induced by the Seebeck effect χ_S . With increasing the chain length n , these two contributions present a first increase which is due to hydrodynamic interactions, and a decrease caused by the counterion condensation. We also observed that, for long chains, the Seebeck term dominates because of its larger hydrodynamic factor χ_S , whereas for short chains the dielectrophoretic term χ_ε prevails. These theoretical results agree with experimental data, in the sense, they both revealed a strong dependence on the molecular-weight and an interesting interplay between hydrodynamic interactions and condensation effect.

Finally, we studied briefly in chapter 5 the time-dependent effect on the dynamics of ions in electrolyte solution. In this chapter, we wanted to know at which time scale ions diffuse once a non-uniform temperature gradient is present. Solving the charge conversation equation and applying the Debye-Hückel approximation, we found the non-stationary thermoelectric field with the characteristic time scale for ion-diffusion $\tau_{\text{ion}} = \lambda^2/D \sim 1\mu\text{s}$, which is, from comparison, much more greater than both hydrodynamic and thermal time scales. At the end of this chapter, we studied the time-dependent effect on particle's slip-velocity which consists of

two contributions: The time-dependent thermoelectric and thermo-osmotic slip-velocity, $v_s^{\text{el}}(t)$ and $v_s^{\text{osm}}(t)$, which set in on the ion-diffusion time scale $\tau_{\text{ion}} \sim 1\mu\text{s}$ and the heat-diffusion time scale $\tau_{\text{th}} \sim 10\text{nanoseconds}$, respectively. Plotting the time-evolution of this two contributions, one observed the thermoelectric slip-velocity more stronger than the thermo-osmotic one in a first ten microseconds. These above points show the important role playing by the electrolyte Seebeck effect on the thermophoresis mechanism for colloids or polyelectrolytes.

Appendix A

Seebeck effect of an uncharged particle

A.1 Equation for the ionic current

Here we give details for the expression of the ionic current resulting from the motion of the ion-species and the approximation done during the computations. We recall the expression of the current given by each ion-species,

$$\mathbf{J}_{\pm} = -D_{\pm} \left(\nabla n_{\pm} + 2n_{\pm} \alpha_{\pm} \frac{\nabla T}{T} \mp n_{\pm} \frac{e\mathbf{E}}{k_B T} \right). \quad (\text{A.1})$$

If we define the total ionic current $\mathbf{I} = e(\mathbf{J}_+ - \mathbf{J}_-)$, one can find his expression as follows,

$$\mathbf{I} = -e(D_+ \nabla n_+ - D_- \nabla n_-) - 2e \frac{\nabla T}{T} (D_+ n_+ \alpha_+ - D_- n_- \alpha_-) + (D_+ n_+ - D_- n_-) \frac{e^2 \mathbf{E}}{k_B T}. \quad (\text{A.2})$$

It's now important to compute and to linearize the quantities: $D_+ \nabla n_+ - D_- \nabla n_-$, $D_+ n_+ \alpha_+ - D_- n_- \alpha_-$, $D_+ n_+ - D_- n_-$, in order to simplify the expression (A.2). In addition, if we assume that the ions densities n_{\pm} vary weakly from the bulk, that is $n_+ + n_- \approx 2n_0$ and $\rho/e \ll n_0$, one finds the following quantities as,

$$\begin{aligned} D_+ n_+ - D_- n_- &\approx 2Dn_0, \\ D_+ \nabla n_+ - D_- \nabla n_- &\approx D \frac{\nabla \rho}{e}, \\ D_+ n_+ \alpha_+ - D_- n_- \alpha_- &\approx (D_0 (\alpha_+ + \alpha_-) + D (\alpha_+ - \alpha_-)), \end{aligned}$$

where $D = (D_+ + D_-)/2$ and $D_0 = (D_+ - D_-)/2$ with D_{\pm} the diffusion coefficient for positive and negative ion. Inserting these above quantities, the expression of the total current is simplified to,

$$\mathbf{I} = -D \left(\nabla \rho + 2n_0 e (\alpha_+ - \alpha_-) \frac{\nabla T}{T} - 2n_0 e^2 \frac{\mathbf{E}}{k_B T} \right) - 2eD_0 (\alpha_+ + \alpha_-) \frac{\nabla T}{T}. \quad (\text{A.3})$$

Rearranging terms, finally the expression of the total current reads as,

$$\mathbf{I} = -D \left(\nabla \rho + \frac{\varepsilon}{\lambda^2} (S \nabla T - \mathbf{E}) \right), \quad (\text{A.4})$$

where ε the solvent permittivity, $\lambda^2 = \varepsilon k_B T / 2n_0 e^2$ is the Debye screening length and $S = D^{-1} (D_+ \alpha_+ - D_- \alpha_-) k_B / e$ is the Seebeck coefficient.

A.2 Debye-Hückel theory

We start by the equation satisfying by the charge density ρ and the electric field E which result from the expression of the total ionic current in the steady state. Thus putting $\mathbf{I} = 0$, one has

$$\nabla \rho + \frac{\varepsilon}{\lambda^2} (S \nabla T - \mathbf{E}) = 0. \quad (\text{A.5})$$

In order to find out the corresponding charge density ρ and the electric field E , it's more easier to solve the differential equation satisfying by the unknown electrostatic potential by introducing the relation $\mathbf{E} = -\nabla \varphi$ with Gauss's law equation $\rho = \varepsilon \operatorname{div} \mathbf{E}$ into the Eq. (A.5), one has

$$\nabla^2 \varphi - \frac{1}{\lambda^2} (\varphi - S \Delta T) = 0, \quad (\text{A.6})$$

where $\Delta T = T(\mathbf{r}) - T_0$ with $T(\mathbf{r})$ the temperature field given in term of a series multipolar expansion

$$T(\mathbf{r}) = T_0 + \sum_n t_n P_n(c) \frac{a^{n+1}}{r^{n+1}}, \quad (\text{A.7})$$

where $c = \cos \theta$ the cosine of the polar angle. The mean excess temperature $t_0 = q / 4\pi k a$ is determined by the rate of the heat absorption q , the thermal conductivity of the solvent k , and the particle radius a .

The differential equation (A.5) has two solutions: the homogeneous and inhomogeneous part, thus the electrostatic potential has two contributions,

$$\varphi = \varphi_T + \varphi_\sigma. \quad (\text{A.8})$$

The stationary heat equation for the temperature field, $\nabla^2 T = 0$, implies that the divergence of the thermoelectric field vanishes, $\nabla \cdot \mathbf{E} = 0$. The corresponding thermopotential φ_T , first solution of equation (A.6), reads as

$$\varphi_T = -S(T - T_0), \quad (\text{A.9})$$

whereas the second solution is given by the Debye-Hückel potential φ_σ , and results from the equation

$$\nabla^2 \varphi_\sigma = \frac{\varphi_\sigma}{\lambda^2}. \quad (\text{A.10})$$

To solve this equation, we decompose the solution

$$\varphi_\sigma(\mathbf{r}) = \sum_n \varphi_n(r) P_n(\cos \theta), \quad (\text{A.11})$$

in the Legendre polynomial basis $(P_n)_{n \geq 0}$. Inserting into Eq. (A.6), one has to solve the following equation

$$\frac{d^2 \varphi_n}{dr^2} + \frac{2}{r} \frac{d\varphi_n}{dr} - \left(\frac{n(n+1)}{r^2} + \frac{1}{\lambda^2} \right) \varphi_n = 0. \quad (\text{A.12})$$

These kind of equations are solved by Bessel functions, and for spherical particle the general solution is given in term of series expansion

$$\varphi_\sigma(\mathbf{r}) = \sum_{n=0}^{\infty} c_n \frac{k_n(r/\lambda)}{k_n(a/\lambda)} P_n(\cos \theta), \quad (\text{A.13})$$

where $k_n = \sqrt{\frac{2}{\pi x}} K_{n+1/2}(x)$ the modified spherical Bessel function of the second kind. For the sake of notational convenience, we introduce the factor $k_n(a/\lambda)$ such that the radial solutions are normalized at the particle surface $r = a$. The complete electrostatic potential reads as,

$$\varphi = - \sum_{n=0}^{\infty} \left(S t_n \frac{a^{n+1}}{r^{n+1}} + c_n \frac{k_n(r/\lambda)}{k_n(a/\lambda)} \right) P_n(c), \quad (\text{A.14})$$

where $c = \cos \theta$. Now it remains to define the coefficients c_n which depend on the electrostatic boundary conditions used at the particle surface.

A.3 Insulating particle

In the case of an insulating uncharged surface, the particle carries no surface charge then the electrostatic boundary conditions require that the normal component of the electric field vanishes,

$$E_{\perp}(r = a) = 0. \quad (\text{A.15})$$

Taking the radial derivative of the potential at the point $r = a$, the coefficients c_n read as,

$$c_n = St_n(n+1) \frac{\lambda k_n(a/\lambda)}{a k'_n(a/\lambda)},$$

with the dimensionless derivative $k'_n(x) = \partial_x k_n(x)$. In order to simplify the expression of the coefficients c_n , we assume that the particle radius a is much greater than one Debye length, $\lambda \ll a$. With this assumption, we expand in term of series λ/a the corresponding function

$$\frac{k_n(r/\lambda)}{k_n(a/\lambda)} = \frac{a}{r} e^{(a-r)/\lambda} \left[1 + \frac{\lambda n(n+1)}{a} \left(1 - \frac{a}{r}\right) + \dots \right].$$

Thus the first terms of the series are well approximated by

$$\frac{k_n(r/\lambda)}{k_n(a/\lambda)} \approx \frac{a}{r} e^{(a-r)/\lambda} \quad (n < \sqrt{a/\lambda}).$$

In the most relevant near-field range, this approximation is even valid for $n < a/\lambda$. To leading order in the small parameter λ/a , we have $k'_n(a/\lambda)/k_n(a/\lambda) = -1 + O(\lambda/a)$. Then the above coefficients read as,

$$c_n = St_n(n+1) \frac{\lambda}{a}. \quad (\text{A.16})$$

The electrostatic potential, final solution of the differential equation (A.6), reads as

$$\varphi = -S \sum_n t_n P_n(c) \left(\frac{a^{n+1}}{r^{n+1}} - (n+1) \frac{\lambda}{r} e^{(a-r)/\lambda} \right). \quad (\text{A.17})$$

The screened term is by a factor λ/a smaller than the first one; yet their radial derivatives cancel each other at $r = a$, thus satisfying (A.15).

With the relation $\mathbf{E} = -\nabla\varphi$, the normal component of the electric field reads, to leading order in λ/a ,

$$E_{\perp}(\mathbf{r}) = S\nabla_{\perp}T(\mathbf{r})(1 - e^{(a-r)/\lambda}). \quad (\text{A.18})$$

In the screened terms we have discarded factors of a/r , since they are close to unity in the range where the exponential function is finite. This explicit how the thermocharge screens the normal electric field. The parallel field component, on the contrary, is hardly affected by the thermocharge,

$$E_{\parallel}(\mathbf{r}) = S\nabla_{\parallel}T(\mathbf{r})(1 + O(\lambda/a)). \quad (\text{A.19})$$

The thermocharge density follows from Gauss' law, $\rho_T = -\varepsilon\nabla^2\varphi_{\sigma}$. With the same approximations as for the normal field component above, we have

$$\rho_T = -\frac{\varepsilon}{\lambda}e^{(a-r)/\lambda}S\nabla_{\perp}T|_S. \quad (\text{A.20})$$

Integrating over the radial coordinate we find the charge per unit area

$$\sigma = \int_0^{\infty} dr \rho_T = -\varepsilon S\nabla_{\perp}T|_S. \quad (\text{A.21})$$

Integrating over the particle surface gives the total charge

$$Q_T = -4\pi a\varepsilon S t_0, \quad (\text{A.22})$$

which is determined by the isotropic component of the excess temperature.

A.4 Conducting particle

In the case of an conducting surface, the electrostatic boundary conditions impose that, at the particle surface, the parallel component of the electric field vanishes, whereas the normal component is compensated by the surface polarization charge σ_P ,

$$E_{\perp} = \frac{\sigma_P}{\varepsilon}, \quad E_{\parallel} = 0. \quad (\text{A.23})$$

For the surface polarization charge, we write it as the series expansion in the Legendre polynomial basis, $\sigma_P = \sum_n s_n P_n(c)$. Now taking the normal and the

parallel derivative of the electrostatic potential φ , the condition (A.23) enable to determine the coefficients c_n and s_n , to leading order in λ/a ,

$$c_n = St_n, \quad s_n = -\frac{\varepsilon St_n}{\lambda} \quad (n > 0),$$

and because of charge conservation, the isotropic terms read as

$$c_0 = \frac{\lambda}{a} St_0, \quad s_0 = 0.$$

Inserting these coefficients, the electrostatic potential reads as,

$$\varphi = -St_0 \frac{a - \lambda e^{\frac{a-r}{\lambda}}}{r} - S \sum_{n>0} t_n P_n(c) \left(\frac{a^{n+1}}{r^{n+1}} - e^{\frac{a-r}{\lambda}} \right). \quad (\text{A.24})$$

With the same approximation done as in the insulating case and the surface polarization condition $\int_S \sigma_S dS = 0$, the expression of the electrostatic potential becomes

$$\varphi = -St_0 \frac{a - \lambda e^{\frac{a-r}{\lambda}}}{r} - S(T_S - \langle T_S \rangle) \left(1 - e^{\frac{a-r}{\lambda}} \right), \quad (\text{A.25})$$

where T_S the temperature field at the surface and $\langle T_S \rangle$ its mean value. The first term account for the isotropic part of the thermopotential whereas the last term account for the anisotropic thermopotential and for the polarization effect. With the expression of the potential given below, one deduces the expression of the polarization charge

$$\sigma_P = -\frac{\varepsilon}{\lambda} S(T_S - \langle T_S \rangle). \quad (\text{A.26})$$

Before computing the component of the electric field, we approximate that, within the screening layer, the factor $(a/r)^n$ is close to unity, thus we discarded the corresponding factor in the following equation. With this approximation, the normal component of the electric field reads as,

$$E_{\perp}(\mathbf{r}) = S \nabla_{\perp} T(\mathbf{r}) - \frac{S(T_S - \langle T_S \rangle)}{\lambda} e^{\frac{a-r}{\lambda}}, \quad (\text{A.27})$$

and the parallel component,

$$E_{\parallel}(\mathbf{r}) = S \nabla_{\parallel} T \left(1 - e^{(a-r)/\lambda} \right). \quad (\text{A.28})$$

The component E_{\perp} and E_{\parallel} satisfy the boundary conditions in (A.23). Applying Gauss's law, $\rho = -\varepsilon\nabla^2\varphi$, we find the thermocharge density within the same approximation,

$$\rho_P = -\frac{\varepsilon}{\lambda^2}e^{(a-r)/\lambda}S(T_S - \langle T_S \rangle). \quad (\text{A.29})$$

Appendix B

Poisson-Boltzmann theory

Previously, we derived the thermoelectric properties of an uncharged hot colloids in a weak-coupling approximation. Now in the case where the particle carries a surface charge σ and in contact with an electrolyte solution, the electrostatic potential φ_σ is solved by the Poisson-Boltzmann equation

$$\nabla^2 \varphi_\sigma = -\frac{\rho}{\varepsilon} = \frac{k_B T}{e \lambda^2} \sinh \frac{e \varphi_\sigma}{k_B T}. \quad (\text{B.1})$$

This last equation is non-linear and doesn't have an analytical solution in 3-dimensional system. Now if we assume that the particle radius is much larger than the Debye screening length, then the curvature of the surface can be neglected, and the non-linear Poisson-Boltzmann equation can be solved in planar geometry where the Laplace operator reduces to the second derivative with respect to the vertical coordinate z , and the potential is the 1D solution [41]

$$\varphi_\sigma(z) = -\frac{2k_B T}{e} \ln \frac{1 + g e^{-z/\lambda}}{1 - g e^{-z/\lambda}}, \quad (\text{B.2})$$

with the shorthand notation

$$\hat{g} = g e^{-z/\lambda}, \quad g = \sqrt{1 + \ell^2/\lambda^2} - \ell/\lambda.$$

The parameter g is given by the ratio of the Gouy-Chapman length ℓ and the Debye length λ ,

$$\ell = \frac{e}{2\pi\ell_B|\sigma|}, \quad \lambda = \frac{1}{\sqrt{8\pi\ell_B n}}.$$

Here we use the Bjerrum length ℓ_B , the surface charge density σ , and the salinity n . In the following we assume a negative surface charge $-\sigma$.

Taking the perpendicular derivative $d\varphi/dz$, the normal electric field reads

$$E_{\perp} = -\frac{\sigma}{\varepsilon} e^{-z/\lambda} \frac{1-g^2}{1-\hat{g}^2}. \quad (\text{B.3})$$

This field is perpendicular to the particle, and it satisfy the relation $E(0) = -\sigma/\varepsilon$.

The charge density in the diffuse layer is readily obtained from Gauss' law $\rho = \varepsilon dE/dz$,

$$\rho = \frac{\sigma}{\lambda} e^{-z/\lambda} \frac{(1-g^2)(1+\hat{g}^2)}{1-\hat{g}^2}. \quad (\text{B.4})$$

Integrating over z one finds

$$\int_0^{\infty} dz \rho(z) = \sigma, \quad (\text{B.5})$$

which means that the counterions ρ completely screen the surface charge density $-\sigma$.

The Debye-Hückel approximations is obtained by taking the limit of small surface charge, where $\ell/\lambda \gg 1$ and $g = \frac{1}{2}\lambda/\ell$, resulting in

$$\varphi_{\sigma} = -\frac{\sigma\lambda}{\varepsilon} e^{-z/\lambda}, \quad E_{\perp} = -\frac{\sigma}{\varepsilon} e^{-z/\lambda}, \quad \rho = \frac{\sigma}{\lambda} e^{-z/\lambda}.$$

Appendix C

Polarization charge

Here we are in the case of a charged conducting surface with an electrolyte solution. The mobile electrons in the metal move until the resulting polarization charge σ_P the double layer potential which is treated within the Poisson-Boltzmann theory. In order to determine σ_P , we begin by assuming that the polarization charge is much more smaller than the uniform surface charge σ_0 , then we expand the Poisson-Boltzmann potential in linear order

$$\varphi_\sigma = \varphi_{\sigma_0} + \sigma_P \frac{d\varphi_{\sigma_0}}{d\sigma_0}, \quad (\text{C.1})$$

where $\sigma = \sigma_P + \sigma_0$ the unknown surface charge.

Taking the parallel gradient of the above equation, one obtains

$$\nabla_{\parallel}\varphi_\sigma = \nabla_{\parallel}\varphi_{\sigma_0} - \frac{\nabla_{\parallel}\sigma_P}{\sigma_0} \frac{2k_B T}{e\sqrt{1+b^2}}, \quad (\text{C.2})$$

where $b = l/\lambda$ the ratio of the Gouy-Chapman length l and the Debye length λ . The electrostatic boundary conditions impose that the gradient vanishes at the surface $\nabla_{\parallel}\varphi_\sigma(z=0) = 0$, thus solving for σ_P we obtain

$$\frac{\nabla_{\parallel}\sigma_P}{\sigma_0} = -\frac{e}{2k_B T} \sqrt{1+b^2} (S\nabla_{\parallel}T - \nabla_{\parallel}\varphi_{\sigma_0}). \quad (\text{C.3})$$

In this last equation, one has to compute the parallel gradient of the Poisson-Boltzmann potential with the uniform surface charge. Thus we have at $z = 0$,

$$\nabla_{\parallel}\varphi_{\sigma_0} = \zeta \frac{\nabla_{\parallel}T}{T} - \frac{4k_B T}{e} \frac{\nabla_{\parallel}g}{1-g^2}, \quad (\text{C.4})$$

where ζ the potential at the particle surface. Note that, in this last equation the Gouy-Chapman length $l = e/2\pi l_B |\sigma_0|$ is given with the uniform surface charge. The last term in Eq. (C.4) result in

$$\frac{\nabla_{\parallel} g}{1-g^2} = -\frac{1}{4\sqrt{1+b^2}} \left(\frac{\nabla_{\parallel} \varepsilon}{\varepsilon} + \frac{\nabla_{\parallel} T}{T} \right),$$

then the equation (C.4) becomes,

$$\nabla_{\parallel} \varphi_{\sigma_0} = \zeta \frac{\nabla_{\parallel} T}{T} + \frac{k_B T}{e} \frac{1}{\sqrt{1+b^2}} \left(\frac{\nabla_{\parallel} \varepsilon}{\varepsilon} + \frac{\nabla_{\parallel} T}{T} \right). \quad (\text{C.5})$$

Inserting this in Eq. (C.3), we obtain finally the surface charge σ_P in Poisson-Boltzmann theory as,

$$\nabla_{\parallel} \sigma_P = -\frac{e\sigma_0 \sqrt{1+b^2}}{2k_B T} \left(S \nabla_{\parallel} T - \zeta \frac{\nabla_{\parallel} T}{T} \right) + \frac{1}{2} \left(\frac{\nabla_{\parallel} \varepsilon}{\varepsilon} + \frac{\nabla_{\parallel} T}{T} \right),$$

With the permittivity gradient $\nabla \varepsilon = (d\varepsilon/dT) \nabla T$. The integral gives

$$\sigma_P = -\sigma_0 \left(\frac{e\sqrt{1+b^2}}{k_B T} (ST - \zeta) - \frac{d \ln \varepsilon}{d \ln T} - 1 \right) \frac{T_S - \langle T_S \rangle}{2T}. \quad (\text{C.6})$$

The last factor follows from the condition of charge neutrality,

$$\langle \sigma_P \rangle = \frac{1}{S} \int_S \sigma_P dS = 0.$$

In the Debye-Hückel limit, the Gouy-Chapman length is large as compared to the Debye length, $b = l/\lambda \gg 1$. Expanding in first order in b^{-1} , we find the surface polarization charge in Debye-Hückel approximation as,

$$\sigma_P = \frac{\epsilon S}{\lambda} (T_S - \langle T_S \rangle). \quad (\text{C.7})$$

Appendix D

Time dependent Seebeck effect

Here we give the details of calculation of the thermoelectric properties in a non-stationary state for a half-metal heated Janus colloid. We consider here an uncharged particle and we assume that the Debye screening length λ is much more smaller than the particle radius a . We start by giving the behavior of the temperature profile around the heated particle. The result of the following section is taken from the paper in Ref. [56].

D.1 Temperature field

The Janus particle of radius a is centered at $\mathbf{r}=0$, its lower hemisphere is coated by a thin metal layer with the conductivity k_C which is considered to be much higher than both of the particle k_p and the surrounding fluid k (taken to be equal for simplicity $k \approx k_p$). We therefore assume that the cap is held at constant temperature $T_0 + \delta T$, with T_0 the bulk temperature. Important to note that the temperature profile remain always in the stationary state because of half metal absorption.

Let $T_l = (T(\mathbf{r}) - T_0) / \delta T$ be the reduced temperature field and solution of the stationary heat equation,

$$\nabla^2 T_l = 0, \tag{D.1}$$

with the mixed boundary conditions

$$\partial_r T_l \Big|_{a^+} = \partial_r T_l \Big|_{a^-}, \quad 0 \leq \theta \leq \pi/2, \tag{D.2}$$

$$T_l(a) = 1, \quad \pi/2 \leq \theta \leq \pi. \quad (\text{metal side}) \tag{D.3}$$

The solution of the Eq. (D.1) in the liquid phase ($r > a$) is

$$T_l(r, \theta) = \sum_{n=0}^{\infty} t_n P_n(\cos \theta) \left(\frac{a}{r}\right)^{n+1}, \quad (\text{D.4})$$

and inside the particle ($r < a$), one finds

$$T_l(r, \theta) = \sum_{n=0}^{\infty} t_n P_n(\cos \theta) \left(\frac{r}{a}\right)^n, \quad (\text{D.5})$$

where P_n the Legendre polynomial and the coefficients t_n are given by

$$t_{2k} = -t_{2k+1} = \frac{(-1)^k}{\pi(2k+1)}, \quad (\text{D.6})$$

except for the first coefficient which reads as, $t_0 = 1/2 + 1/\pi$.

D.2 Conservation equation

We start by the charge conservation characterizing the creation and diffusion of the ionic current inside and outside the screening layer. This equation is satisfied by the electric charge density $\rho = e(n_+ - n_-)$, with n_{\pm} the ions densities, and the total ion current $\mathbf{I} = e(\mathbf{J}_+ - \mathbf{J}_-)$,

$$\frac{\partial \rho}{\partial t} + \text{div } \mathbf{I} = 0. \quad (\text{D.7})$$

The expression of the total current \mathbf{I} , given in appendix A, is obtained within the Debye-Hückel approximation, and by applying Gauss's law, $\rho = \varepsilon \text{div } \mathbf{E}$, his expression becomes

$$\mathbf{I} = -\varepsilon D \left(\nabla^2 \mathbf{E} - \frac{1}{\lambda^2} (\mathbf{E} - S \nabla T) \right). \quad (\text{D.8})$$

In the simple way, the conservation equation can be written only in function of the unknown electric field E . For that, we apply again the Gauss equation, so one has

$$\nabla \cdot (\partial_t \mathbf{E}) = \nabla \cdot \left\{ D \left(\nabla^2 \mathbf{E} - \frac{1}{\lambda^2} (\mathbf{E} - S \nabla T) \right) \right\}. \quad (\text{D.9})$$

In this last equation, the left and right hand sides functions depend on the same variables, thus it can be simplified as

$$\partial_t \mathbf{E} = D \left(\nabla^2 \mathbf{E} - \frac{1}{\lambda^2} (\mathbf{E} - S \nabla T) \right). \quad (\text{D.10})$$

where $D = (D_+ + D_-) / 2$ the sum of ion diffusion coefficient.

This partial differential equation modelizes the distribution of the generated electric field inside the system in the non-stationary state. The right hand side characterizes the term of reaction and the left hand side the term of diffusion. When $\partial_t E = 0$, we find the same differential equation as in section A.2 where the system is in steady state.

We want here to solve the Eq. (D.10) and find out the generated electric field and the ion diffusion time scale which characterizes the time of creation of the Seebeck field. To have simple computations, the problem is reduced to solve the differential equation satisfying by the reduced electrostatic potential ψ according to $\mathbf{E} = -S\delta T \nabla \psi$.

Inserting this last relation to Eq.(D.10), one has to solve the following equation,

$$\frac{\partial \psi}{\partial t} = D \left(\nabla^2 \psi - \frac{1}{\lambda^2} (\psi - T_l) \right). \quad (\text{D.11})$$

For further, we assume that the Debye screening length λ is much more smaller than the particle radius a . When we consider that the particle carries no surface charge, thus the normal component of the electric field vanishes at the surface. As a consequence, the resulting electrostatic boundary conditions reads as,

$$\mathbf{n} \cdot \nabla \psi = 0, \quad \text{for } r = a, \quad (\text{D.12})$$

where \mathbf{n} the normal unit vector perpendicular to the particle surface.

D.3 Method of resolution

The differential equation (D.11) with its boundary condition (D.12) given above depend in space and in time. To solve these kind of equations, one of the best way is to apply the Laplace transform where the time derivative is replaced by the function, $s\psi$, where ψ is the function Laplace transform of the electric potential and s an variable in the Laplace space.

With this transformation, the Eq. (D.11) becomes

$$\nabla^2 \tilde{\psi} - \left(\frac{s}{D} + \frac{1}{\lambda^2} \right) \tilde{\psi} = \frac{T_l}{\lambda^2 s}. \quad (\text{D.13})$$

Now this last equation is solved by the method of direct solution. In this case, the electrostatic potential consists of two contributions,

$$\tilde{\psi} = \tilde{\psi}_h + \tilde{\psi}_T, \quad (\text{D.14})$$

where the thermopotential (inhomogeneous part) reads as,

$$\tilde{\psi}_T = s^{-1} (1 + s\tau_{\text{ion}}) T_l, \quad (\text{D.15})$$

where the parameter,

$$\tau_{\text{ion}} = \frac{\lambda^2}{D}, \quad (\text{D.16})$$

characterizes the ion diffusion time scale or relaxation time for the creation of the thermoelectric field.

The homogeneous part $\tilde{\psi}_h$ is well described by the Debye-Hückel equation,

$$\nabla^2 \tilde{\psi}_h = \left(\frac{s}{D} + \frac{1}{\lambda^2} \right) \tilde{\psi}_h. \quad (\text{D.17})$$

In the previous sections, it has been shown that the general solution of this last equation is the usual modified spherical Bessel functions. Thus we obtain,

$$\tilde{\psi}_h = \sum_n \tilde{c}_n(s) \frac{k_n(r\sqrt{1+s\tau_{\text{ion}}}/\lambda)}{k_n(a\sqrt{1+s\tau_{\text{ion}}}/\lambda)} P_n(\cos\theta). \quad (\text{D.18})$$

With the assumption $a \gg \lambda$, the modified Bessel functions k_n can be simplified and developed in term of λ/a in the following way,

$$\frac{k_n(r\sqrt{1+s\tau_{\text{ion}}}/\lambda)}{k_n(a\sqrt{1+s\tau_{\text{ion}}}/\lambda)} = \frac{a}{r} e^{\frac{(a-r)}{\lambda}\sqrt{1+s\tau_{\text{ion}}}} \left[1 + \frac{\lambda}{a} \frac{n(n+1)}{2\sqrt{1+s\tau_{\text{ion}}}} \left(1 - \frac{a}{r} \right) + \dots \right],$$

where the first terms of the series are well approximated by,

$$\frac{k_n(r\sqrt{1+s\tau_{\text{ion}}}/\lambda)}{k_n(a\sqrt{1+s\tau_{\text{ion}}}/\lambda)} \approx \frac{a}{r} e^{\frac{(a-r)}{\lambda}\sqrt{1+s\tau_{\text{ion}}}} \quad (n < \sqrt{a/\lambda}).$$

In order to find the coefficients \tilde{c}_n in the Laplace space, as in previous sections we apply the boundary condition (D.12). To leading order in λ/a , we find

$$\tilde{c}_n(s) = -(n+1) \frac{\lambda}{a} \frac{t_n}{s(1+s\tau_{\text{ion}})}. \quad (\text{D.19})$$

Thus the function Laplace transform of the reduced electrical potential completely reads as,

$$\tilde{\psi}(\mathbf{r}, s) = \sum_n \left\{ \left(\frac{a}{r}\right)^{n+1} - (n+1) \frac{\lambda}{r} e^{\frac{(a-r)}{\lambda} \sqrt{1+s\tau_{\text{ion}}}} \right\} \frac{t_n P_n(\cos \theta)}{s(1+s\tau_{\text{ion}})}. \quad (\text{D.20})$$

To find the original function, we must compute the inverse Laplace transform of Eq. (D.20). Here, the inverse transform is very difficult to calculate because of the presence of the square root. To overcome this difficulty, we approximate that $s\tau_{\text{ion}} \ll 1$, and to leading order in λ/a we find finally

$$\psi(\mathbf{r}, t) = \psi(\infty) (1 - e^{-t/\tau_{\text{ion}}}), \quad (\text{D.21})$$

where the function,

$$\psi(\infty) = \sum_n t_n P_n(\cos \theta) \left(\frac{a^{n+1}}{r^{n+1}} - (n+1) \frac{\lambda}{r} e^{(a-r)/\lambda} \right), \quad (\text{D.22})$$

is the reduced electrostatic potential in the steady state.

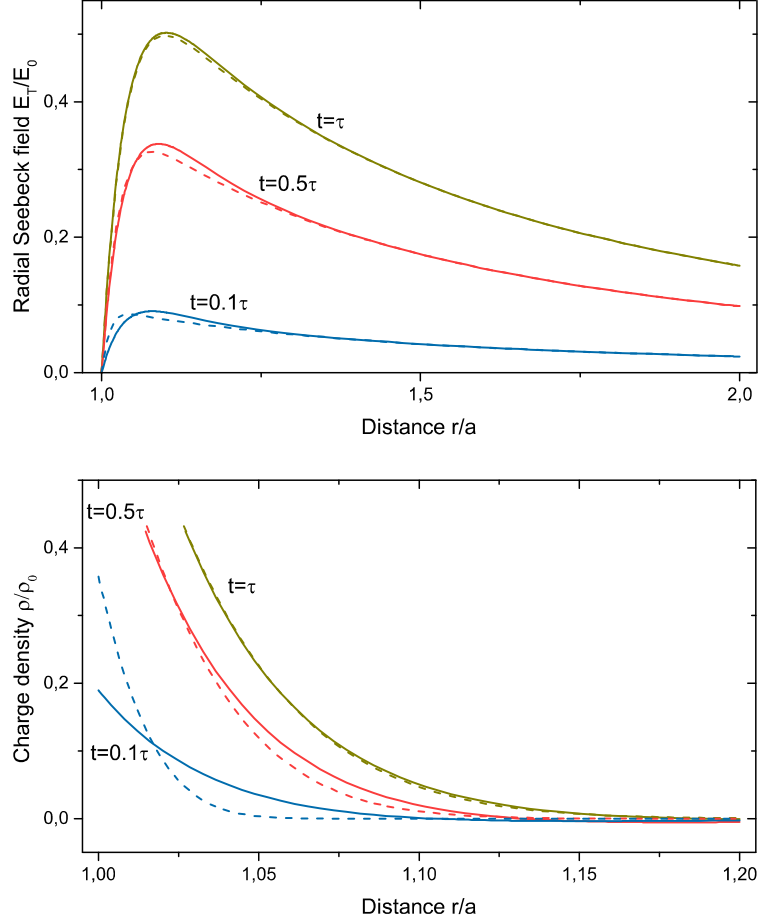


Figure D.1: The radial thermoelectric field \mathbf{E}/E_0 and charge density ρ/ρ_0 , with $E_0 = -S\delta T/a \sim 30\text{KV/m}$ and $\rho_0 = -S\epsilon\delta T/\lambda(a + \lambda) \sim 571.43 \times 10^{-3}\text{V}/\mu\text{m}^2$, in function of the radial distance r/a at three different times scale. The relaxation time is about $\tau = 0.0025\text{s} = 2.5\text{ms}$ then we have taken the interval of time as $t \in [0.1\tau, \tau]$ with the following parameters: the excess temperature $\delta T = 30\text{K}$, the diffusion coefficient $D = 1\mu\text{m}^2/\text{s}$, the Seebeck coefficient $S = -10^{-3}\text{V/K}$, and the Debye length $\lambda = 50\text{nm}$. The dashed line and the continuous line in these graph represent, respectively, the numerical inversion for the Laplace transform based on the Talbot's method and the approximate analytical solution. This numerical computation has been done in order to validate the approximation solution resulting from the invers Laplace transform.

Remerciements

Je veux exprimer mes remerciements et ma gratitude à toutes les personnes qui m'ont apporté l'aide et l'assistance nécessaire à l'élaboration de cette thèse.

Avant tout d'abord, j'adresse mes remerciements les plus grands et les plus sincères à mon superviseur Prof. Alois Würger pour avoir accepté de m'encadrer pour ce travail ainsi qu'à ses orientations, sa disponibilité, ses précieux conseils et sa confiance. Durant toute la thèse, j'ai beaucoup appris de lui, de la façon dont il aborde et résout les problèmes en physique de manière simple, de son sens du travail, et de son humilité. Avec toutes les difficultés que j'ai pu rencontrer durant les trois années d'études, il a su m'apporter l'aide nécessaire avec de la patience jusqu'à la réalisation de ce travail.

Je tiens aussi à remercier tout le Laboratoire (LOMA) pour l'agréable séjour, l'administration, toute l'équipe physique théorique, mes collègues de travail: Goce, Mathieu et Marcela pour leur amitié et toutes autres personnes avec qui j'ai pu passer trois belles années au LOMA.

Un grand merci s'adresse aussi à ma famille pour leur patience et pour m'avoir toujours soutenu et encouragé tout au long de mes études. Je ne saurais terminer sans remercier Mme Isabelle Guillaume pour son aide dans toutes mes démarches administratives.

Merci à tous et que Dieu nous accorde sa bénédiction, nous donne la santé, longue vie, la paix et la réussite totale dans nos projet future.

Bibliography

- [1] J. L. Anderson, *Annu. Rev. Fluid Mech.* **21**, 61 (1989).
- [2] J.C. Giddings, F.J. Yang, M.N. Myers, *Flow Field Fractionation: a versatile new separation method*, *Science* **193**:1244-1245 (1976).
- [3] B. Abécassis, C. Cottin-Bizonne, C. Ybert, A. Ajdari, L. Bocquet, *Nature materials* **10**, 1038 (2008).
- [4] M. Braun and F. Chichos, *ACS Nano* **12**, 11200-11208 (2013).
- [5] S. Duhr and Dieter Braun, *Phys. Rev. Lett* **97**, 038103 (2006).
- [6] B. V. Derjaguin, G. P. Sidorenkov, E. A. Zubashchenkov, and E. V. Kiseleva, *Kolloidn. Zh.*, **9**, 335 (1947).
- [7] J. P. Ebel, J. L. Anderson, D. C. Prieve, *Ame. Chem. Soc.*, **88**, 0743-7463 (1987).
- [8] B. V. Derjaguin, N. V. Churaev, V. M. Muller, *Surface Forces*, Plenum Press, New York (1987).
- [9] M. Von Smoluchowski, *Phys. Z.*, **6**, 530 (1905).
- [10] H.J. Keh and J.L. Anderson, *J. Fluid. Mech.* **153**, 417-439 (1985).
- [11] E. Ruckenstein, *J. Colloid Interface Sci.* **83**, 77 (1981).
- [12] J. C. Giddings et *al.*, *Macromolecules* **9**, 109 (1976).
- [13] P. -G. de Gennes, *Scaling concepts in Polymer Physics*, Cornell University Press: Ithaca (1979).

- [14] B. V. Derjaguin and G. P. Sidorenkov, Dokl. Akad. Nauk SSSR **32**, 622 (1941).
- [15] S. Simoncelli, J. Summer, S. Nedev, P. Kühler, and J. Feldmann, Small **29**, 2854 (2016).
- [16] A. Eslahian, Argya Majee, Micheal Maskos, Alois Würger, Soft Matter Royal Society of Chemistry **10**, 1931 (2014).
- [17] D. Vigolo, S. Buzzaccaro, R. Piazza, Langmuir **26**, 7792 (2010).
- [18] A. Würger, Phys. Rev. Lett. **101**, 108302 (2008).
- [19] S. A. Putnam, D. G. Cahill, Langmuir **21**, 5317 (2005).
- [20] J. L. Viovy, Rev. Mod. Phys. **72**, 813 (2000).
- [21] H. A. Stone et al, Annu. Rev. Fluid Mech. **36**, 381 (2004).
- [22] S.S. Dukhin and B.V. Derjaguin, *Surface and Colloid Science*, edited by E. Matijevic (Wiley, New York, 1974).
- [23] H.A. Stone et al, Annu. Rev. Fluid Mech. **36**, 381 (2004).
- [24] B. Abécassis et al., Nature Mat. **7**, 785 (2008).
- [25] F. Brochard and P. -G. de Gennes, C. R. Acad. Sc. Paris., Série 2 **293**, 1025 (1981).
- [26] B. Derjaguin and G. Sidorenkov, Dokl. Acad. Nauk SSSR **32**, 622 (1941).
- [27] M. Muthukumar, Macro. Theo. Simul. **3**, 61-71 (1994).
- [28] M. Muthukumar, Electrophoresis **17**, 1167-1172 (1996).
- [29] Argya Majee, Doctoral thesis, Université de Bordeaux (2012).
- [30] J. N. Agar et al, J. Phys. Chem. **93**, 2082 (1989).
- [31] J. N. Agar, in *Advances in Electrochemistry and Electrochemical Engineering* Vol. 5, ed. by P. Delahay (Interscience, New York, 1963).
- [32] A. Würger, Rep. Prog. Phys. **73**, 126601 (2010).

- [33] T.M. Squires and S.R. Quake, *Rev. Mod. Phys.* **77**, 977 (2005).
- [34] P.E.J. Rouse, *J. Chem. Phys.* **21**, 1272-1280 (1953).
- [35] B.H. Zimm, *J. Chem. Phys.* **24**, 269-278 (1956).
- [36] H. Cottet, P.Gareil, O.Theodoly, C. Williams, *Electrophoresis* **21**, 3529-3540 (2000).
- [37] K. Grass, U. Böhme, U. Scheler, H. Holm, *Phys. Rev. Lett.* **100**, 096104 (2008).
- [38] H.R Jiang, N. Yoshinaga, M. Sano, *Phys. Rev. Lett* **105**, 268302 (2010).
- [39] S. Nedev, S. Carretero-Palacios, P. Kühler, T. Lohmüller, A.S. Urban, L.J.E. Anderson and J. Feldmann, *ACS Photonics* **2**, 491-496 (2015)
- [40] A. Majee, and A. Würger, *Phys. Rev. Lett.* **108**, 118301 (2012)
- [41] D. Andelman, In *Soft Condensed Matter Physics in Molecular and cell Biology*, Poon, W., Andelman, D. (eds.), Scottish Graduate Series (Taylor and Francis 2006)
- [42] T.M. Squires and M.Z. Bazant, *J. Fluid Mech.* **509**, 217 (2004)
- [43] D. Stadelmaier, W. Köhler, *Macromolecules* **41**, 6205 (2008)
- [44] M. Reichl, M. Herzog, A. Götz, and D. Braun, *Phys. Rev. Lett.* **112**, 198101 (2014)
- [45] A.P. Bregulla, A. Würger, K. Günther, M. Mertig, and F. Cichos, *Phys. Rev. Lett.* **116**, 188303 (2016)
- [46] H.-R. Jiang, H. Wada, N. Yoshinaga and M. Sano, *Phys. Rev. Lett.* **102**, 208301 (2009)
- [47] T. Tsuji, K. Kozai, H. Ishino, and S. Kawano, *Micro & Nano Letters*, doi: 10.1049=mn.2012.0357 (2017)
- [48] M. Braibanti, D. Vigolo, R. Piazza, *Phys. Rev. Lett.* **100**, 108303 (2008).
- [49] A. Würger, *Phys. Rev. Lett.* **116**, 138302 (2016).

- [50] K. Grass and C. Holm, *Faraday Discuss.* **144**, 57-70 (2010)
- [51] J. Morthomas and A. Würger, *Eur. Phys. J.* **27**, 425-434 (2008)
- [52] S. Kim, S. J. Karilla, *Microhydrodynamic: Principles and Selected Applications*, Butterworth-Heinemann Boston (1991)
- [53] G. S. Manning, *J. Chem. Phys.* **51**, 924 (1969) and *J. Phys. Chem.* **85**, 1508-1515 (1981)
- [54] A. Sim, J. Lipfert, D. Herschlag, S. Doniach, *Phys. Rev. E.* **86**, 021901 (2012)
- [55] M. Reichl, M. Herzog, A. Götz, D. Braun, Supplemental material (2014)
- [56] T. Bickel, A. Majee, A. Würger, *Phys. Rev. E* **88**, 02301 (2013)